Master Thesis
TVVR 17/5005

Numerical Simulation of Saltwater Intrusion Caused by Land-Use Change and Groundwater Pumping in a Salinity-Affected Coastal Aquifer, Japan

Keisuke Konishi

Division of Water Resources Engineering
Department of Building and Environmental Technology
Lund University

Numerical Simulation of Saltwater Intrusion Caused by Land-Use Change and Groundwater Pumping in a Salinity-Affected Coastal Aquifer, Japan

By:
Keisuke Konishi

Master Thesis

Division of Water Resources Engineering
Department of Building & Environmental Technology
Lund University
Box 118
221 00 Lund, Sweden

Water Resources Engineering
TVVR-17/5005
ISSN 1101-9824

Lund 2017
www.tvrl.lth.se

Master Thesis
Division of Water Resources Engineering
Department of Building & Environmental Technology
Lund University

English title:	Numerical Simulation of Saltwater Intrusion Caused by Land-Use Change and Groundwater Pumping in a Salinity-Affected Coastal Aquifer, Japan
Author(s):	Keisuke Konishi
Supervisor:	Ronny Berndtsson
Examiner:	Magnus Persson
Language	English
Year:	2017
Keywords:	Saltwater intrusion, Land-use change, Groundwater pumping, Groundwater recharge model, three-dimensional density dependent solute transport model

Acknowledgements

This paper is a product of my academic experiences and lessons throughout my master course at the Division of Water Resources Engineering, Lund University and the Institute of Urban and Environmental System Engineering Faculty of Engineering, Kyushu University.

I am deeply grateful to my supervisor Associate Professor Yoshinari Hiroshiro for giving me a significant support and plenty of advice. I got a lot of knowledge about groundwater from him and could not have finished this research without his guidance.

From Lund University, Professor Ronny Berndtsson helped me a lot when I was in Lund University. He cared about me after I came back to Japan. I really appreciate his help.

I am also grateful to Atsushi Tsutsumi in SG Technical Consultant Corporation for giving me invaluable advice about groundwater recharge model. He came to Kyushu University all the way once a month and discussed my research. I could get a lot of ideas from the discussions.

Edangodage Duminda Pradeep Perera provided me with density dependent solute transport model. Without his help this paper would not have been possible.

Finally, I would like to appreciate all my colleagues for discussions and helping me in the lab.

Abstract

Lowering of groundwater level may cause saltwater intrusion in coastal aquifers. Since decrease in groundwater recharge rate and overpumping lower groundwater level, recharge rate and pumping rate are main factors of saltwater intrusion In the study area, the land-use has been changing since a university campus was newly constructed. Therefore, there is concern that this rapid land-use change will increase the extent of saltwater intrusion in this area. The main aim of this thesis is to evaluate the effects of land-use change which decreases recharge rate, and groundwater pumping on saltwater intrusion. The simulations are conducted in different cases to compare those effects. The two models, groundwater recharge model and three dimensional density dependent solute transport model are applied to calculate salinity concentrations. The simulation results show that higher groundwater pumping rate enhances more saltwater intrusion than the land-use change. This is because the recharged water in the surrounding area prevents drastic lowering of groundwater level. Furthermore, the decrease in recharge rate due to the land-use change lowers groundwater level uniformly in the whole area, which maintains the seaward hydraulic gradient and velocities. This thesis can be used to prevent saltwater intrusion in this study area in the future.

Table of Contents

1. Introduction

1.1. Background

Groundwater has been one of the largest sources of water for agriculture, business and drinking in many parts of the world. Although groundwater is important water resource, human activities have become a threat for the sustainability of groundwater. In many countries, contamination of groundwater caused by human activities is becoming a very serious problem.
Saltwater intrusion, which is the movement of fresh-saltwater interface into freshwater aquifer, has been identified as a major problem which occurs in coastal aquifers in many countries. Due to the difference between the densities of freshwater and saltwater, freshwater is found above saltwater and prevents the upward movement of saltwater. However, in some situations, the interface of freshwater and saltwater, which is also called zone of dispersion, moves into freshwater aquifer. As shown in Figure 1.1, groundwater flow can be seen in both freshwater and saltwater zones. Freshwater flows towards the sea and saltwater flows towards the freshwater aquifer. The position of the fresh-saltwater interface can be influenced by change in groundwater level according to the Ghyben-Herezberg principle.

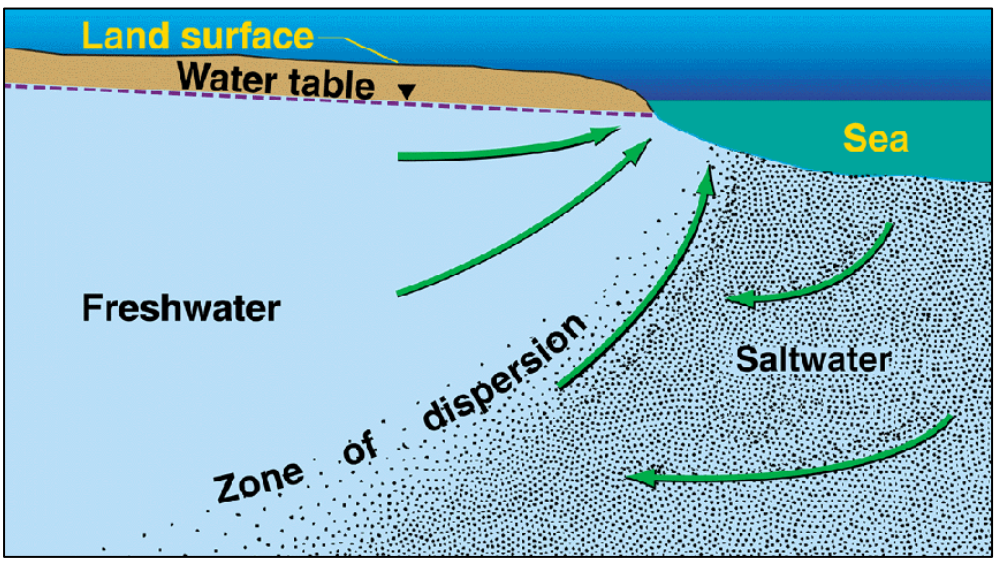

Figure 1.1 Groundwater flow near the fresh-saltwater interface (Barlow, 2003)

The Ghyben-Herezberg principle states that in unconfined aquifers the depth to the fresh-saltwater interface below sea level is approximately 40 times the freshwater level above sea level under steady state conditions (Figure 1.2).

This principle is determined by the difference between the densities of freshwater and saltwater;

$$z = \frac{\rho_f}{\rho_s - \rho_f} h \quad (1)$$

where z is the height of freshwater level above sea level, and h is the depth to the fresh-saltwater interface below sea level. ρ_f and ρ_s are the densities of freshwater and saltwater, respectively.

Generally, the densities of freshwater and saltwater are 1.000 g/cm^3 and 1.025 g/cm^3, respectively. Therefore, Equation (1) can be rewritten as;

$$z = 40h \quad (2)$$

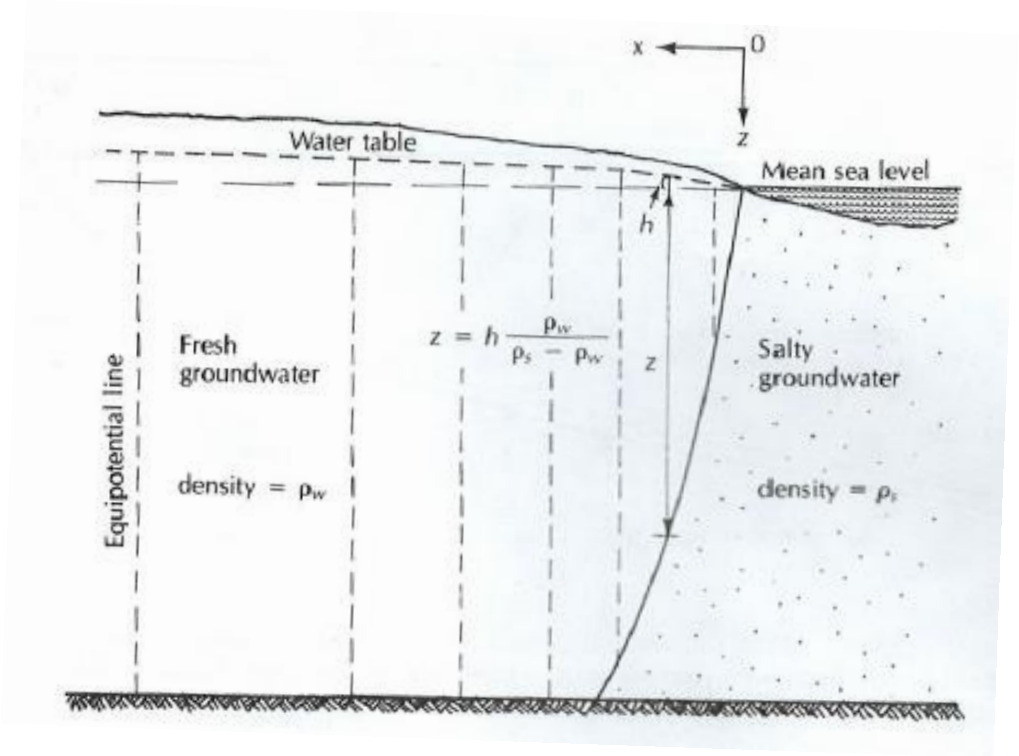

Figure 1.2 Relationship between freshwater level above sea level and the depth to the fresh-saltwater interface below sea level (Fetter, 2001)

According to the principle, lowering of groundwater level would cause the movement of the fresh-saltwater interface into freshwater aquifer. Lowering of groundwater level takes place when the demanding groundwater discharge exceeds the groundwater recharge, so that groundwater discharge and groundwater recharge are key factors for saltwater intrusion. In many parts around the world, saltwater intrusion caused by high rates of groundwater pumping was reported. High rates of groundwater pumping can have a great

impact on groundwater level. Although the major cause of saltwater intrusion is over pumping of groundwater, an effect of lowered groundwater recharge rate on saltwater intrusion cannot be ignored (Barlow, 2010).

Groundwater is used in different ways; domestic, agricultural and industrial use. Amounts of required groundwater discharge depend on the way groundwater is used. For example, much amount of water is required in areas where irrigation and greenhouses are very active. If there are no large rivers and lakes, groundwater would be very valuable water source for those activities.

Amounts of groundwater recharge depend on several factors, such as precipitation, temperature and land-use. Since groundwater originally comes from precipitation, amounts of groundwater recharge increase with more precipitation. Higher temperature increases evapotranspiration, resulting in a decrease in groundwater recharge rate. Besides climate conditions, land-use also influences recharge rates. According to Mccuen (2004), the runoff coefficient, which is surface runoff divided by rainfall,changes with surface types as shown in Table 1.1. The table demonstrates unimproved areas such as farmland or mountain area have higher recharge rates than business and residential area. Since precipitation amount is mainly divided into evapotranspiration, surface runoff and groundwater recharge, an amount of groundwater recharge decreases with larger surface runoff.

Table 1.1 Runoff coefficients for different land-use (McCuene, 2004)

Description of Area	Range of Runoff Coefficients
Business	
Downtown	0.70-0.95
Neighborhood	0.50-0.70
Residential	
Single-family	0.30-0.50
Multiunits, detached	0.40-0.60
Multiunits, attached	0.60-0.75
Residential(suburban)	0.25-0.40
Apartment	0.50-0.70
Industrial	
Light	0.50-0.80
Heavy	0.60-0.90
Parks, cemeteries	0.10-0.25
Playground	0.20-0.35
Railroad yard	0.20-0.35
Unimproved	0.10-0.30

If salinity level in groundwater rises, groundwater cannot be used in many ways. Since the water quality has a large influence on human health and crop production, there are criteria for different uses. In the guidelines for water quality, there are two common assessments that express salinity level. Salinity level can often be reported in either Total Dissolved Solid (TDS) or Electric Conductivity (EC). Both total dissolved solid and electric conductivity have high correlation with salinity level. The units of TDS and EC are ppm and μS/cm, respectively. TDS also can be expressed as mg/l. Electric conductivity, which is the other widely used salinity measurement method, has become much more useful than TDS because it can be measured instantaneously and easily by farmers in the field. Since salt dissolved in groundwater conduct electricity, the salinity level is directly related to EC.
The relationship between TDS (ppm) and EC (μS/cm) can be expressed as;

$$\mathrm{TDS} = 6.4 \times \mathrm{EC} \qquad (3)$$

The salinity hazard of irrigation water is shown in Table 1.2.

Table 1.2 Salinity hazards for groundwater

Limitation for use	Electric conductivity (μS/cm)
None	≦ 750
Slight	760 – 1500
Moderate	1500 – 3000
Severe	> 3000

(http/www.lenntch.com)

The yield of different crops in relation with the salinity content of water used for irrigation depends on the type of crops, soil and environmental conditions. The selected area of this study is a coastal agricultural area where groundwater pumped up from wells is used for greenhouse farming. The most distinct sign of high salinity level of groundwater is reduction in crop growth and loss in yield. Crops can tolerate salinity up to certain levels without measurable loss in yield. The salinity threshold (ECe) is the maximum average soil salinity a crop can tolerate in the root zone without decline in yield. If the salinity level is higher than the threshold, the crop yield reduces as salinity level increases.
Table 1.3 shows the salinity threshold of the main crops.

Table 1.3 Salinity thresholds for different crops

Crop Name	Average root zone salinity threshold (ECe) in µS/cm
Field Crop	
Cotton	7700.0
Wheat	6700.0
Sunflower	4200.0
Rice	3000.0
Corn grain sweet	1700.0
Sugar cane	1700.0
Fruits	
Olive	4000.0
Peach	3200.0
Grapefruit	1800.0
Orange	1700.0
Grape	1500.0
Apple	1000.0
Vegetables	
Tomato	2300.0
Potato	1700.0
Onion	1200.0

(http/www.lenntch.com)

In order to maintain a sound salinity levels for crop growths when groundwater is used for agriculture in coastal aquifer, good understanding and management are essential.

Motooka area, which is situated in the Itoshima Peninsula of the western part of Fukuoka prefecture, is mainly composed of agricultural areas. However, in recent years land-use has been changing due to the population growth since a new college campus was constructed. Impervious areas such as paved roads or parking lots have increased along the main street to the university campus as shown in Figure 1.3. Under this situation, there is concern that this land-use change will reduce the amount of groundwater recharge and induce saltwater intrusion in the future. Motooka area is located only 900m away

from a bay and groundwater with high salinity level has been observed at some points. Therefore, groundwater users, especially farmers, pay attention to fluctuations of groundwater salinity level.

Figure 1.3 The aerial photographs of Motooka area taken in 2010 (left figure) and 2015 (right figure)

1.2. Objectives

As presented above, high rates of groundwater pumping and low rates of groundwater recharge may trigger saltwater intrusion in coastal aquifers. There are many studies about an effect of groundwater pumping on saltwater intrusion. However, little has been reported on an effect of a decrease in groundwater recharge rate. Hence, in the study area which is subject to rapid land-use change, the land-use change is feared to increase the extent of saltwater intrusion. In view of the above, it is of great importance to simulate saltwater intrusion in the study area to evaluate effects of groundwater pumping and land-use change on that.

Therefore, the main objective of this study is to evaluate the effects of groundwater pumping and land-use change on saltwater intrusion in the study area. Groundwater recharge model and density dependent solute transport model are applied to simulate saltwater intrusion. In the simulation, assumptions of groundwater pumping rates and land-use are changed to compare the effect of groundwater pumping and land-use change on saltwater intrusion.

2. Study area

2.1. Location

The study area is located at the latitude 33 degrees 35.4 minutes north and longitude 130 degrees 13.4 minutes east, and in the Itoshima peninsula of the western part of Fukuoka prefecture, Japan as shown in Figure 2.1. The study area and its environs are called Motooka region. The study area is on a prefectural road to Ito Campus of Kyushu University that is located in the north of the study area. The area is approximately 267,000 m^3. It is the vicinity of Japan Sea and only 900 m away from a bay called Imazu Bay. The elevation of the ground surface ranges from 0.3m above mean sea level at the lowest point to about 26 m above mean sea level at the highest point.

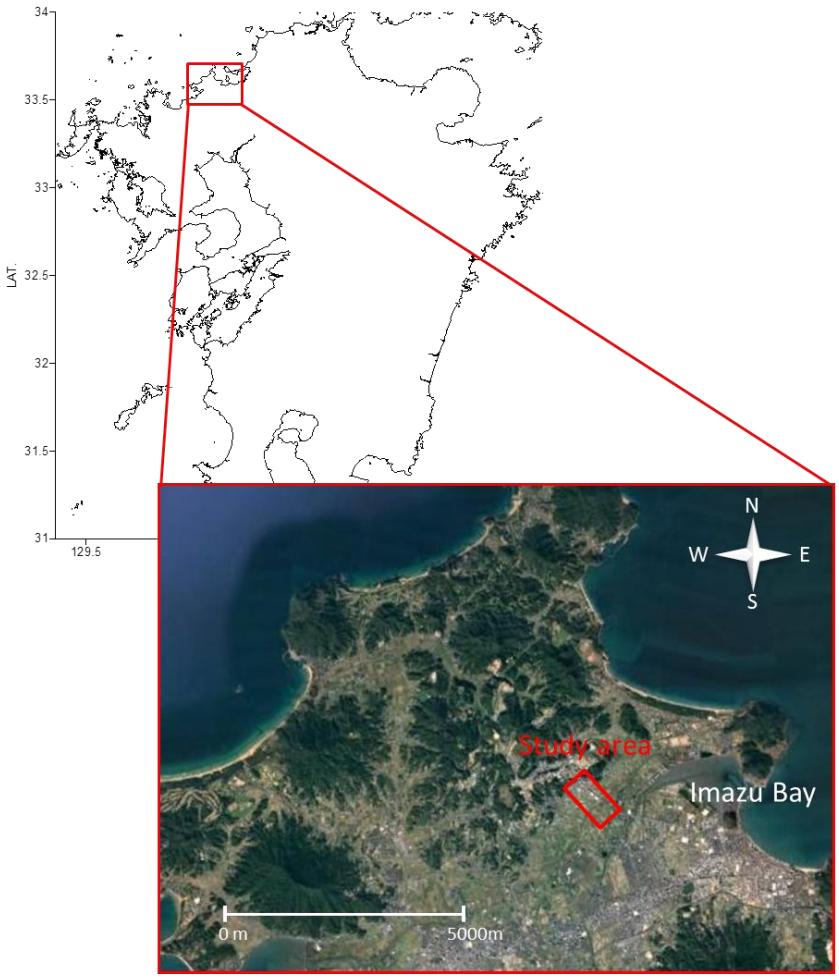

Figure 2.1 Location of the study area

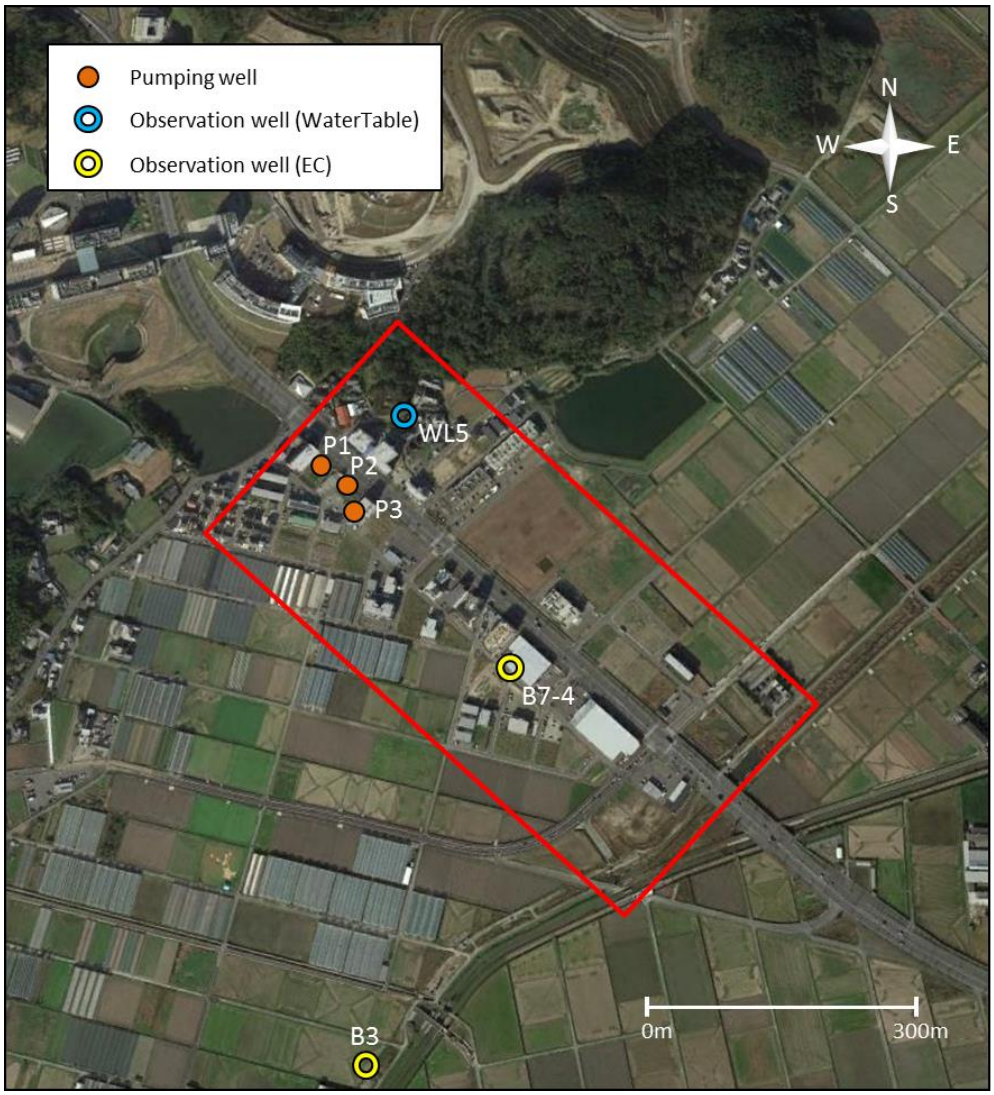

Figure 2.2 Close photo of the study area

2.2. Climate

Climate data is available at the Maebaru weather station on an hourly basis. The maebaru data station is situated at latitude 33 degrees 33.6 minutes north and longitude 130 degrees 11.5 minutes east. The area is characterized as having high humid, large rainfall and high wind speed. The mean annual precipitation for the latest 10 years (from 2005 to 2015) is 1692 mm/year. Figure 2.3 shows that much precipitation occurs from June to August. The mean annual pan potential evaporation is 600 mm/year. The mean annual temperature is 16.5 °C with maximum and minimum of 29.7 and 3.3 °C, respectively.

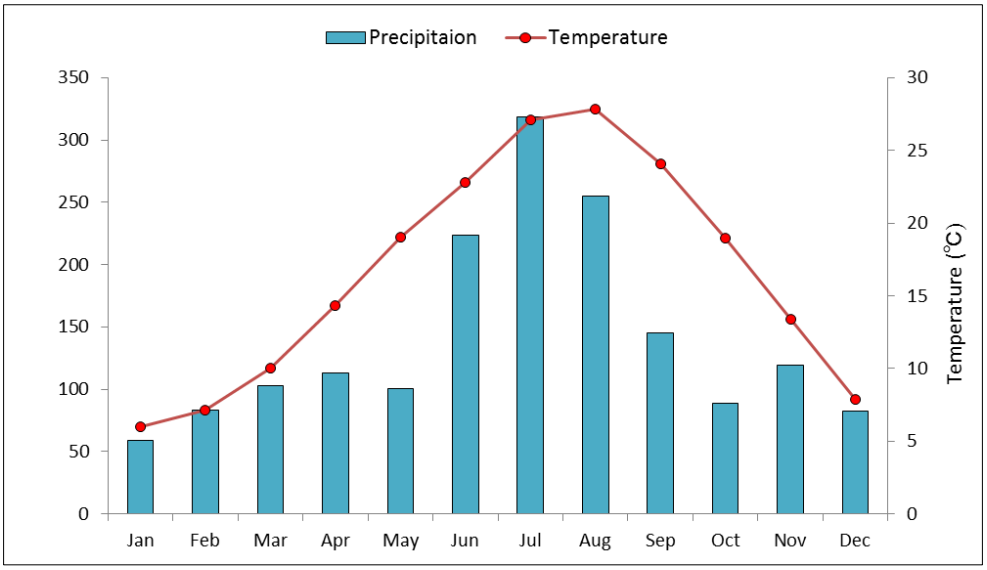

Figure 2.3 Precipitaion and temperature at the maebaru data station

2.3. Geology

Figure 2.4 presents the geological characteristics of the study area and its environs. In the north of the campus, the geological characteristics are divided across the geologic boundary into schist in the north side and granite in the south side. In the study area, the granite is covered with gravel, sand and mud.

Figure 2.5 and 2.6 depict the boring survey position around the campus and soil samples obtained from boreholes in and near the study area. From the result of the boring survey. it is found that the granite is very hard in the deep position but cracks can be seen near the surface. The granite was weathered where the cracks are observed. The weathered granite became decomposed granite at some positions. The decomposed granite is getting thick as it goes to the south and the thickness reaches over 20 m near Mizusaki River. Over the decomposed granite cohesive soils that are impermeable are seen. The cohesive soil is 5-7 m thick at B12 and nearly 1 m thick at B9. It can be considered that the impermeable soil gets thinner as it goes to the mountain. This impermeable soil prevents groundwater in the aquifer from moving upward, which is called an aquiclude. Hence, it is assumed that the study area has an artesian aquifer in the south part and an unconfined aquifer in the north part.

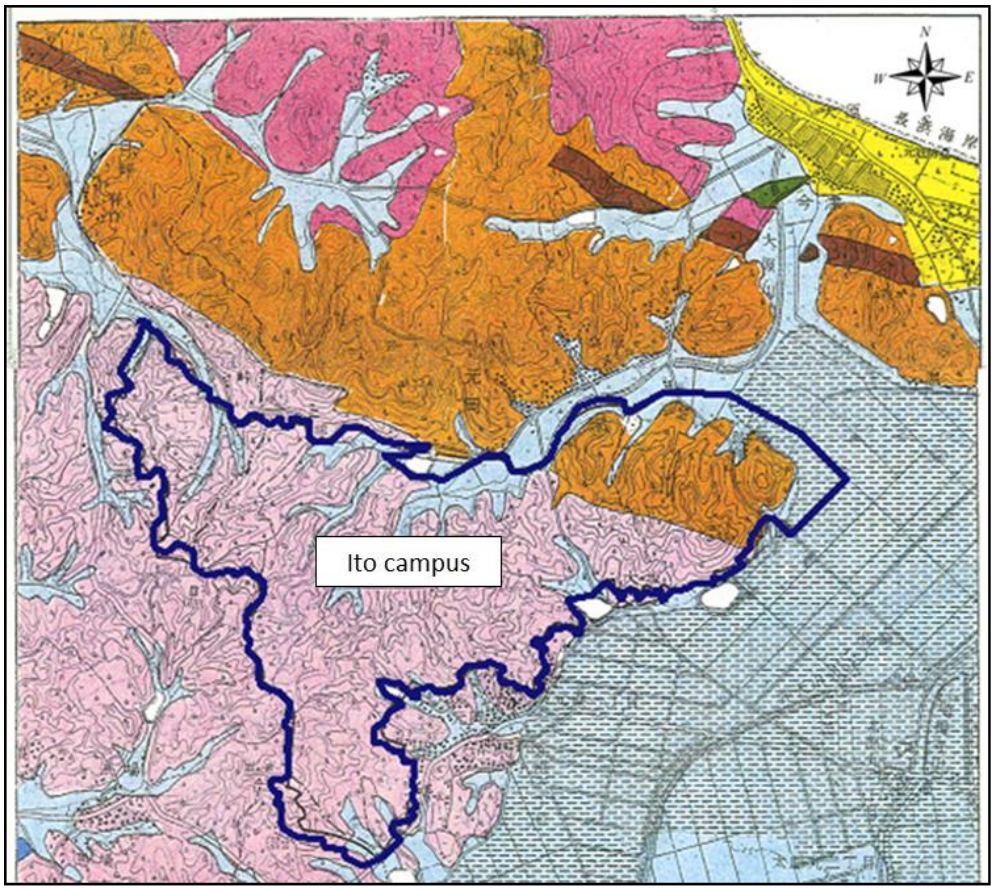

Figure 2.4 Geological characteristics in the study area and its environs

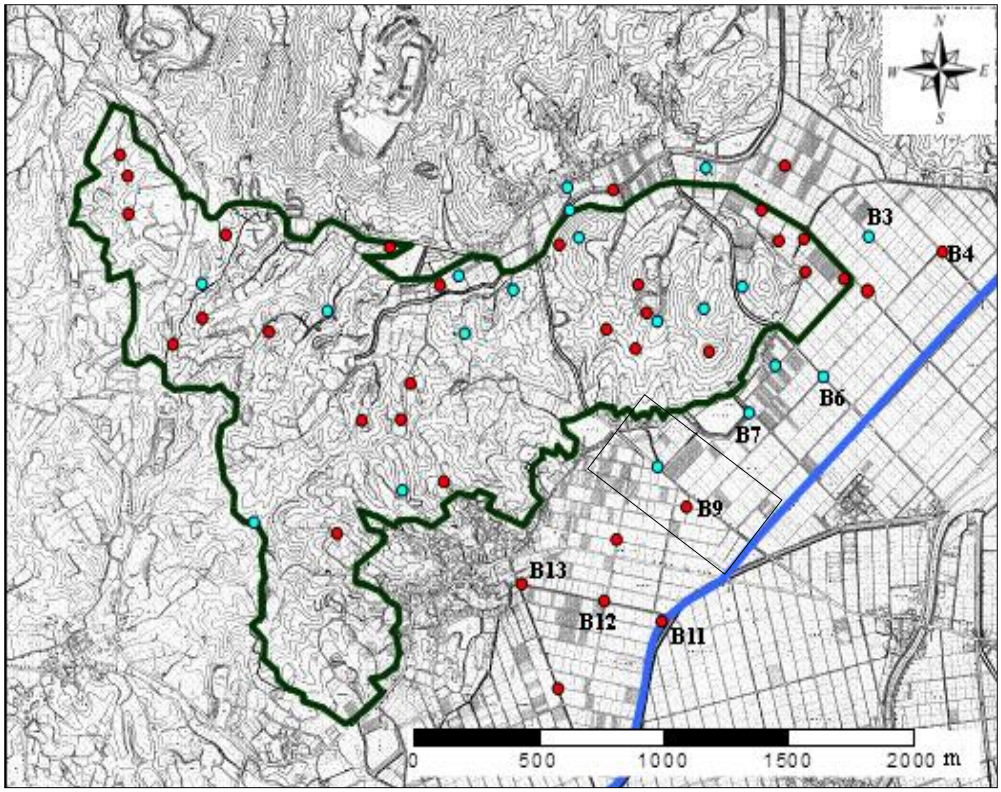

Figure 2.5 Location of the boring survey

B9

B12

Figure 2.6 Soil samples obtained from B9 and B12

2.4 Land-use

Figure 2.7 and 2.8 show the land-use of the study area in 2010 and 2015, respectively. Due to population growth caused by the new campus of Kyushu University, the land-use in Motooka area has been changing. The study area was mainly composed of agricultural areas such as crop fields and greenhouses before 2010. However, a lot of buildings have been constructed where the areas used to be crop fields, so that the impervious area that reduces an amount of groundwater recharge has increased.

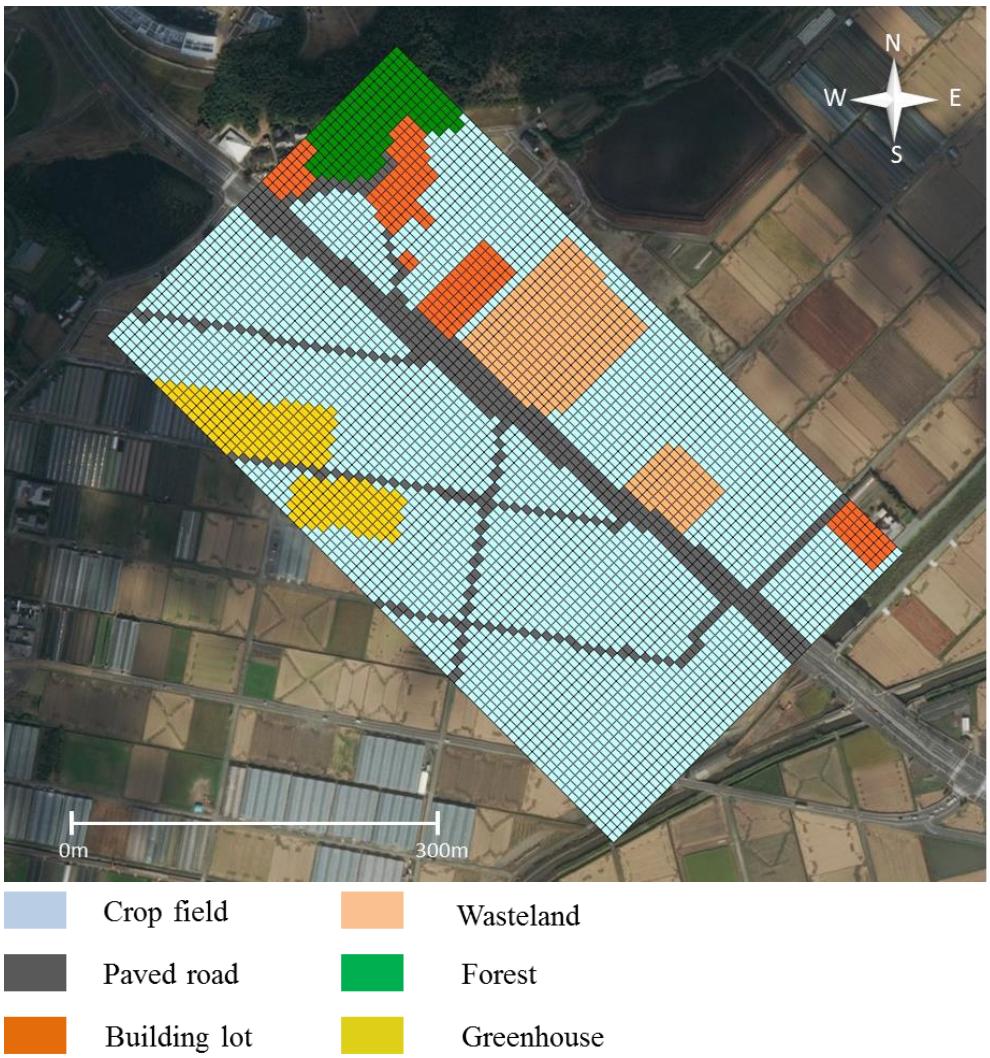

Figure 2.7 Land-use in the study area in 2010

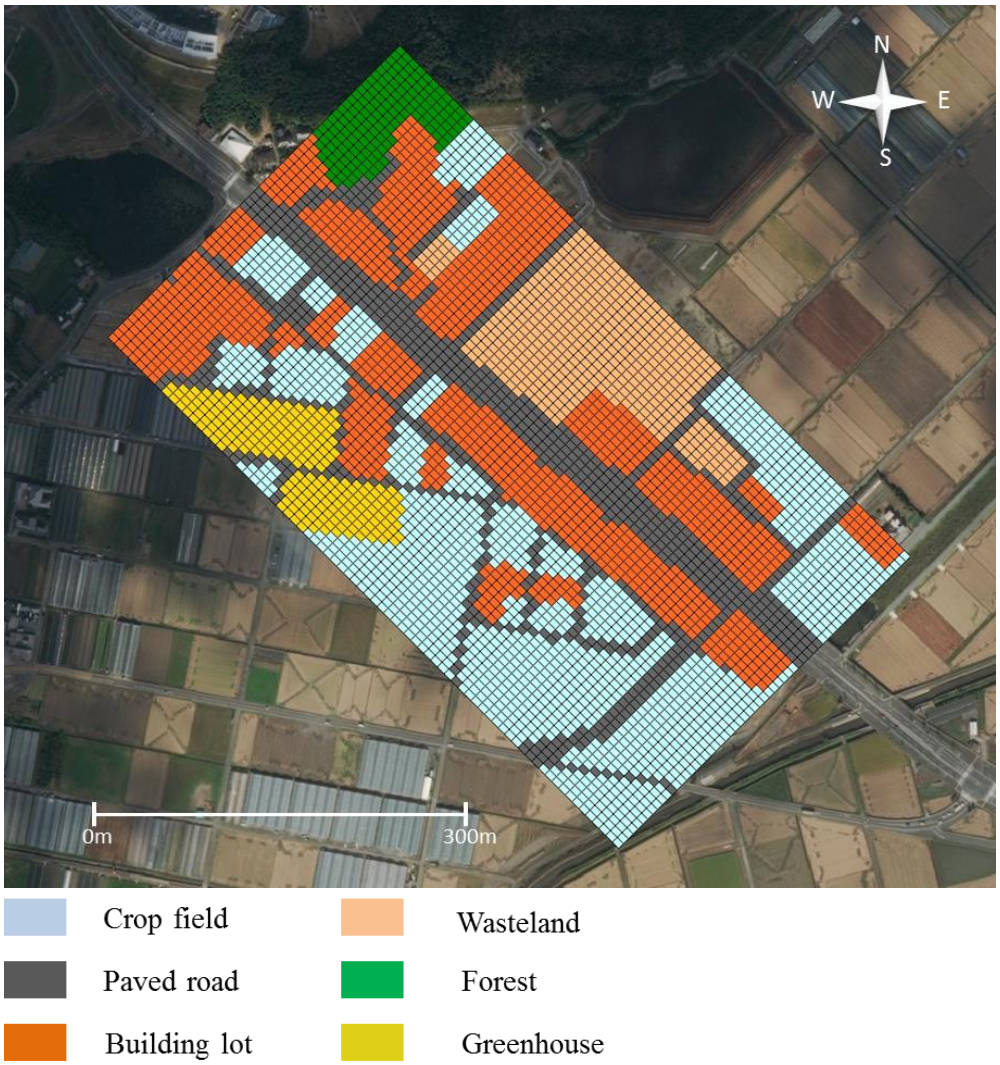

Figure 2.8 Land-use in the study area in 2015

2.5 Observations

In Motooka region, hydrological characteristics have been observed since the construction of Ito campus started in order to keep a careful watch on the influence of the construction. Groundwater level, river water discharge and electric conductivities have been measured. There are 27 groundwater level observation wells, 3 river discharge observation points and 13 electric conductivity observation boreholes. Groundwater level and river discharge are observed on a daily basis and electric conductivity is measured on a monthly basis. Some of them were missed due to road construction but most are still used for the observation.

In the study area, there is one groundwater level observation well (WL5) and one electric conductivity observation borehole (B7-4). The positions of the well and borehole are shown in Figure 2.2. The groundwater level at WL5 is available from 1996 to 2015 and the electric conductivity at B7-4 is available from 2000 to 2010.

2.6 Groundwater utilization

The population has been growing since the campus was constructed, but the people living in the newly constructed apartment or houses get water from a water purification plant. Therefore, groundwater pumped up from the wells is mainly utilized for agriculture in this area. The positions of the wells are shown in Figure 2.2. Since groundwater discharge meters are not attached to the three wells, the amount of groundwater discharge has not been recorded. Hence, the amount of groundwater discharge has to be estimated from available information. In Motooka region, there are 14 pumping wells for agriculture other than the three wells. Out of the 14 wells, water discharge meters are attrached to the 7 wells. the amount of groundwater discharge has been recorded on a monthly basis. According to Kamensky's experiment, well diameter is proportional to an amount of groundwater discharge from a well and therefore an amount of groundwater discharge can be estimated from well diameter and available recorded discharge. Using the recorded amount of discharge from the 7 pumping wells and the well diameter of the three wells in the study area, the amount of groundwater discharge can be roughly estimated. More detailed information about the estimation way is presented by Konishi et al. (2016).

2.7 Groundwater level fluctuation

Figure 2.9 shows groundwater level above MSL at the water level observation well WL5 from 2000 to 2010. This well is used for drinking in a private house and located inside the house. Groundwater level usually ranges from 4 m to 5 m above MSL. After much precipitation, higher groundwater level is observed. Groundwater level is lowered significantly at some points, which is probably caused by groundwater pumping from the near wells.

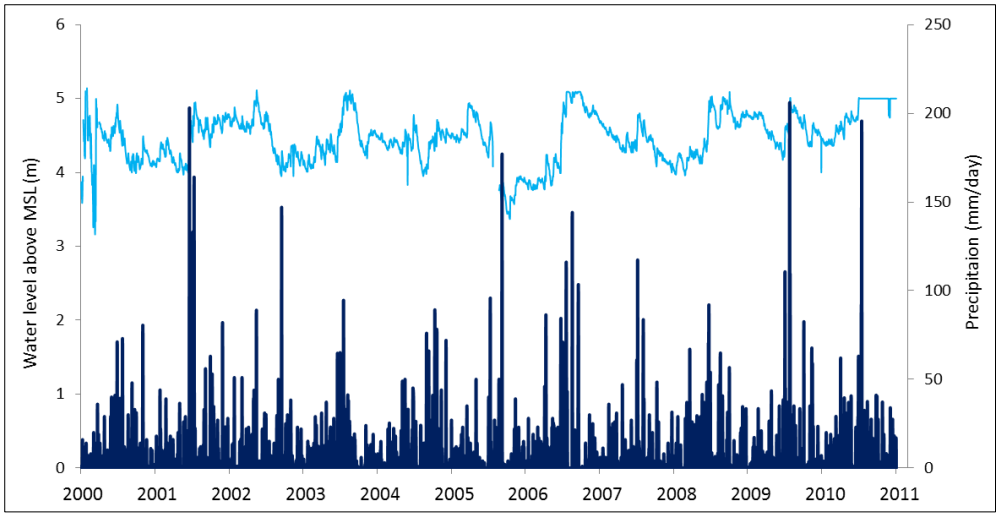

Figure 2.9 Groundwater level at the well WL5 from 2000 to 2010

2.8 Electric conductivity

Figure 2.10 shows the observed electric conductivities at the borehole B7-4 located in the study area from 2005 to 2010. It can be seen from the figure that the electric conductivities change irregularly from 20 m to 30 m depth due to groundwater pumping around the borehole in a year. The interface of freshwater and saltwater can be observed at the depth of 22m to 23m in most of a year but it can be lowered to the depth of 25 m to 27 m in winter. It is considered that the positions of the interfaces are influenced by the amount of groundwater pumping from the wells located around the borehole.

Figure 2.11 shows the observed electric conductivities at the borehole B7-4 and B3. The borehole B3 is located approximately 400 m away from the study area. As shown in Figure 2.2, The borehole B3 is farther from the sea than B7-4. However, up to 20 m depth, the electric conductivity at B3 is considerably higher than that at B7-4. This is because the borehole B3 is very close to Mizusaki River and the river with high salinity level water is losing.

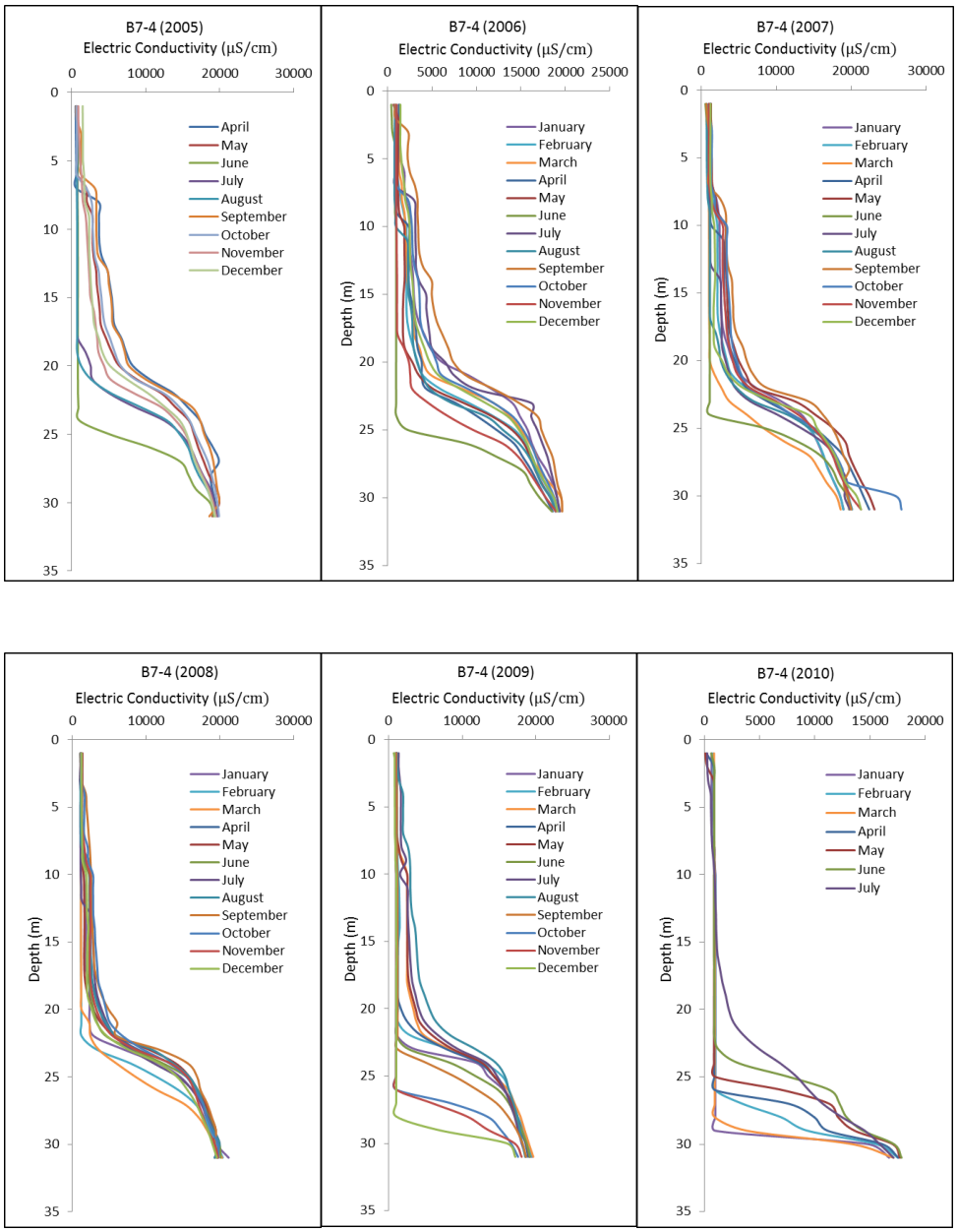

Figure 2.10 Electric conductivities at B7-4 from 2006 to 2010

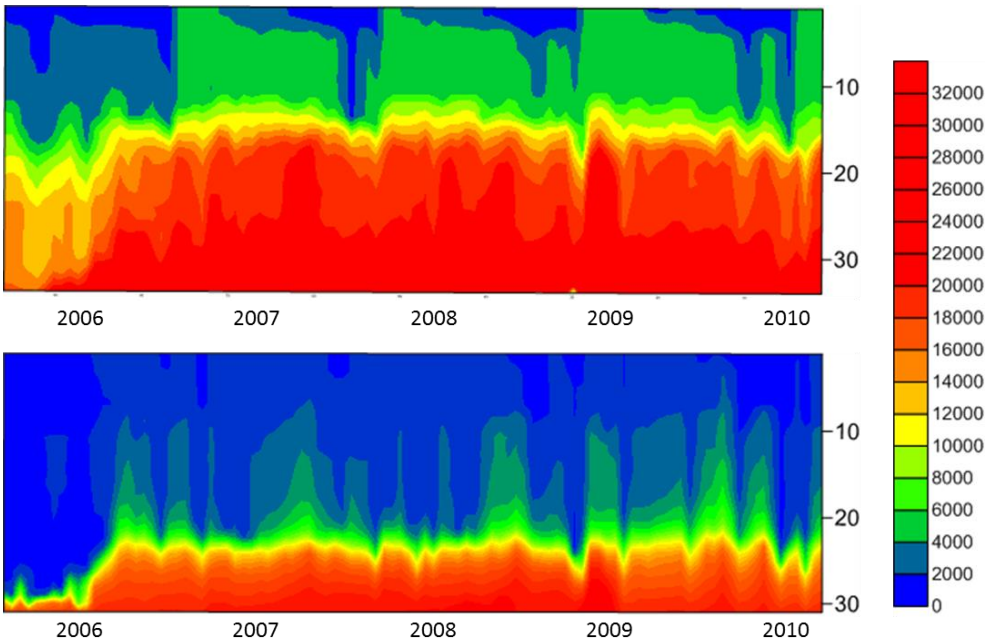

Figure 2.11 Electric conductivities with time at B3 (top figure) and B7-4 (bottom figure)

3. Methodology

3.1. Analysis conditions

The simulations are conducted under to compare the effect of the land-use on saltwater intrusion with that of the groundwater pumping. The simulation period is 26 years from 2005 to 2030, which is divided into two periods; a validation period from 2005 to 2010 and an estimation period from 2011 to 2030 (Table 3.1). The results from the validation period are used for a validation of the model simulation and the ones from the estimation period are used for an evaluation of the effect of the land-use change and groundwater pumping on saltwater intrusion.

In the validation period the simulation starts in the same condition which can mirror the reality of that period. Afterwards, the three cases have different conditions in the estimation period. The set of assumptions adopted for the simulation in the estimation period.

- The meteorological conditions are maintained as observed in 2012-2015.
- In Case 2, the ratio of impervious surface is assumed to increase at the rate of 29.8 percent for five years. This ratio of increase in impervious surface is determined by the aerial photographs of the study area taken in 2010 and 2015. It is assumed that the impervious surface will increase at the same pace after 2015.
- In Case 3, the groundwater pumping rate is doubled in the whole estimation period. According to the recoded groundwater discharge at the other wells in Motooka region, there is a big variation on a yearly basis. The doubled amount was observed at some of the wells and therefore the pumping rate is assumed to be doubled.

Table 3.1 Analysis conditions

<table>
<tr><th colspan="2"></th><th>Validation Period</th><th colspan="3">Estimation Period</th></tr>
<tr><td rowspan="3">Ratio of impervious surface</td><td>Case 1</td><td rowspan="3">14.8%</td><td colspan="3">14.8%</td></tr>
<tr><td>Case 2</td><td>44.6%</td><td>74.4%</td><td>100%</td></tr>
<tr><td>Case 3</td><td colspan="3">14.8%</td></tr>
<tr><td rowspan="3">Pumping rate</td><td>Case 1</td><td rowspan="3">$10m^3/d$</td><td colspan="3">$10m^3/d$</td></tr>
<tr><td>Case 2</td><td colspan="3">$10m^3/d$</td></tr>
<tr><td>Case 3</td><td colspan="3">$20m^3/d$</td></tr>
</table>

The two models, groundwater recharge model and three dimensional density dependent solute transport model, are used. The recharge model is applied to

estimate groundwater level at the borders of the study area and groundwater recharge rates from the surface in the whole area. The simulated groundwater level and recharge rates are used as input data for the solute transport model. The next section presents conceptual model, mathematical model and numerical model.

3.2. Conceptual model

As shown in Figure 3.1, the simulation model domain is divided into three geological regions according to the boring survey. The three geological regions are named as aquiclude, aquifer and bedrock. The aquiclude is assumed to be a confining layer. The hydraulic conductivity is assigned to each geological region.

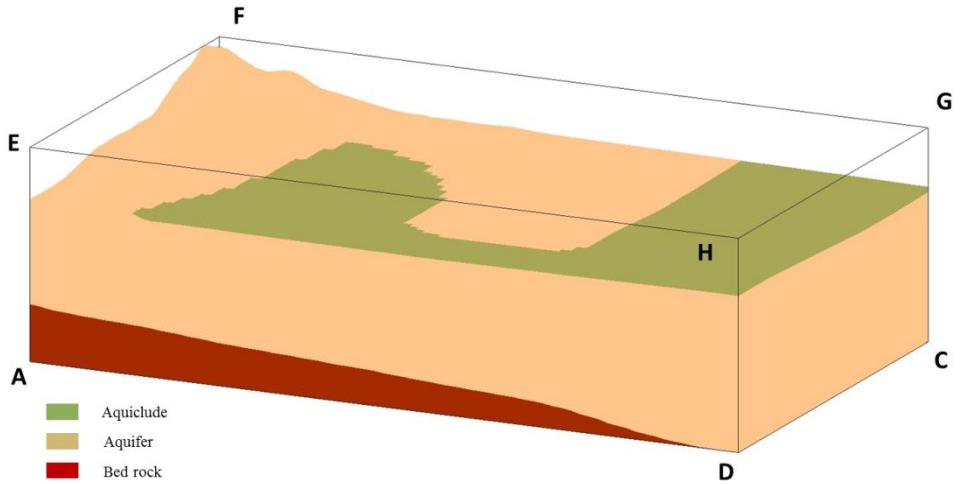

Figure 3.1 Categorization of the geological regions

Boundary conditions are assigned to the 6 boundaries; 4 vertical boundaries, top boundary and bottom boundary. The salinity levels at the borders are assumed that the southern boundary has the same salinity level as seawater and the northern boundary has the same salinity level as freshwater. Groundwater recharge takes place at the surface boundary and no flow boundary is assigned to the bottom boundary.

The three pumping wells are located in the northern part of the model region. Figure 3.2 shows the cross-section view of the model region with the pumping wells. The pumping wells P1, P2 and P3 are positioned 36 m, 90 m and 108 m away from the northern boundary, respectively. The depths of borings are until 24 m from the bottom of the model region and the well screen ranges from 24 m to 40 m from the bottom for the three wells. No

information is found about the screen of the three wells, so the depths of the screens are determined by the previous study (Perera, 2010).

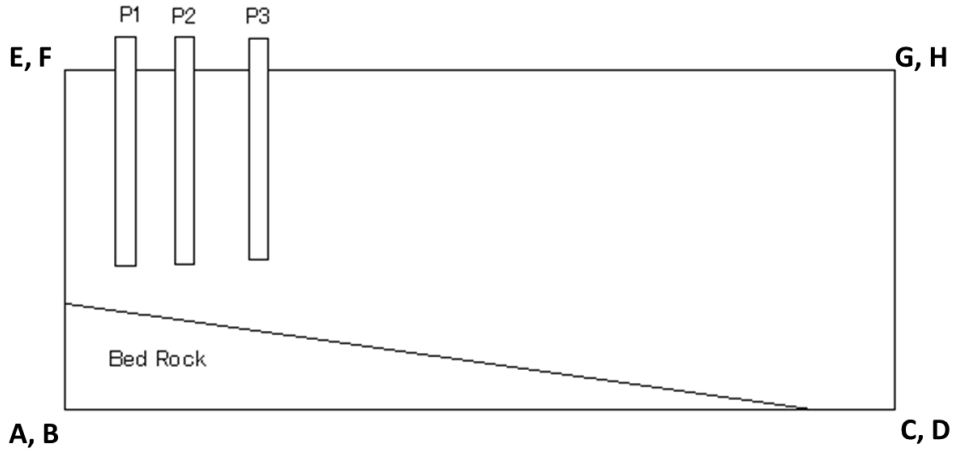

Figure 3.2 Cross-section view of the pumping wells

3.3. Mathematical model

3.3.1. Groundwater recharge model

Since groundwater recharge is one of the main factors to simulate the effect of land-use change on saltwater intrusion, the accurate groundwater recharge needs to be required. In order to estimate groundwater recharge rates and groundwater table at boundary of the selected area, the groundwater recharge model linked to the quasi three-dimensional two-phase groundwater flow model (Tsutsumi et al.,2004) is applied. This section presents how groundwater recharge rates and groundwater levels are calculated.

Figure 3.3 illustrates the groundwater recharge model. This model functions as a vertical tank storage with an outlet at height R_0 and an outlet coefficient a_L that controls outflow from the tank. The R_0 represents the soil field capacity and a_L controls the groundwater recharge rate $q_w(t)$ from the tank. In addition, $r_{int}(t)$ represents the rainfall interception and rainfall that reaches the ground surface r(t) the difference between $r_{total}(t)$ and $r_{int}(t)$, which is described as $r(t) = r_{total}(t) - r_{int}(t)$, where $r_{total}(t)$ is the total rainfall intensity. When there is no tree in areas, $r(t) = r_{total}(t)$.

After the interceptions by trees, the rainfall that reaches the ground surface is divided into two components: the surface runoff and the infiltration. The surface runoff rate is given as $F(r)\cdot r(t)$ and the infiltration rate is $[1 - F(r)]\cdot r(t)$, where F(r) is the surface runoff coefficient as a function of rainfall intensity.

$EVT_1(t)$ denotes evapotranspiration that reduces water stored in the tank.. Additional evapotranspiration can be caused by water uptake which is represented as $EVT_2(t)$ from the groundwater table through the unsaturated zone and the root zone if the water in the tank gets empty (Bouwer, 1978). This phenomena take place when the vertical distance between the ground surface and the groundwater table is less than the extinction depth Hg* in the unconfined aquifer. Anderson & Woessner (1992) introduced a similar approach that takes into account water uptake rate from the groundwater as a linear function of the water table depth below Hg*. Hence, the total evapotranspiration can be assumed to be the sum of $r_{int}(t)$, $EVT_1(t)$ and $EVT_2(t)$. The change in tank water level $h_w(t)$ is calculated as Equation (1) and the recharge rate to the unconfined groundwater aquifer is described as Equation (2) as below.

$$\frac{dh_w}{dt} = \{1 - F_i(r)\} \cdot r(t) - q_w(t) - EVT_1(t) \quad (1)$$

$$q_w(t) = a_L \cdot \{h_w(t) - R_0\} \times Y[h_w(t) - R_0] \quad (2)$$

where $Y\{h_w(t) - R_0\}$ is a step function which equals to 1 for $h_w(t) > R_0$ and 0 for $h_w(t) < R_0$. $q_w(t)$ is the recharge rate from surfaces to groundwater system. The four model parameters $F_i(r)$, a_L, R_0 and n_e used for Equation (1) and (2) need to be determined. The surface runoff coefficient $F_i(r)$ is a function of hourly rainfall intensity as seen in Equation (3). In this equation, the ground surface condition decides the parameter $F_{i\infty}$ which corresponds to the surface runoff coefficient. For example, a typical value of $F_{i\infty}$ is close to 0.3 for forest areas and close to 0.8 for asphalt areas (Ven Te Chow, 1964). Table 3.2 shows the values of $F_{i\infty}$ used in Japan.

$$F(r) = \frac{r(t)}{r(t) + (r)_{1/2}} \cdot F_{i\infty} \quad (3)$$

where $(r)_{1/2}$ is represented as the value of r(t) when $F_i(r)$ becomes $F_{i\infty}/2$.

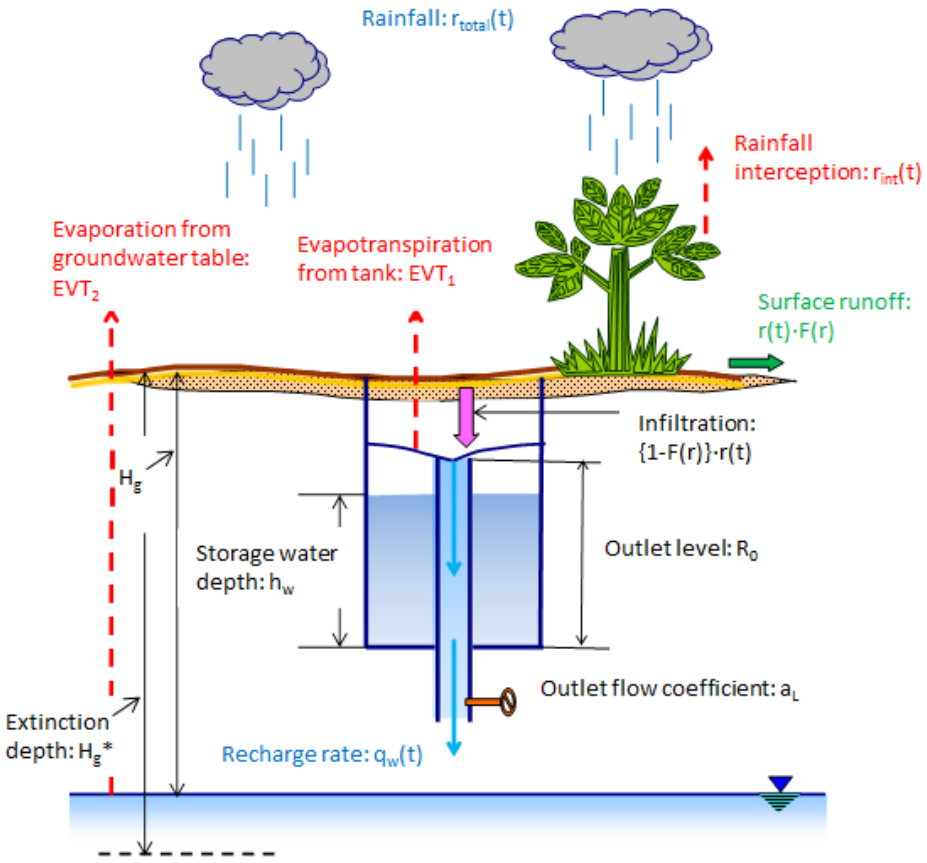

Figure 3.3 Illustration of groundwater recharge model (Tsutsumi et al, 2004)

Parameter estimation

Parameters need to be determined from the available information about rainwater infiltration. The amount of information increases as the number of groundwater observation wells increases. The reaction of groundwater level to rainfall at each well can be used to determine parameters. The parameters may have to be adjusted if the variation in groundwater table at observation wells is not accurately simulated. Nevertheless, this way of parameter estimation requires much calculation effort and may give reliable parameters.
Assuming that significant horizontal groundwater flow does not take place until infiltrated water reaches groundwater table, it is possible to identify the parameters used in the groundwater recharge model independently The estimation way of the four unknown parameters in the groundwater recharge model is described below. The outlet level R_0 is determined by the groundwater table at a certain observation well. R_0 is assumed to be the maximum value of the total precipitation which is not large enough to induce a significant rise in the groundwater table. The effective porosity n_e is

evaluated and determined by dividing the groundwater recharge by the observed the groundwater level fluctuation for a certain rainfall event. The other parameters can be determined by minimizing the function J in Equation (4):

$$J = \sqrt{\sum_{t=1}^{N} \frac{\left[h_{fobs}(i,t) - h_{fcal}(i,t)\right]^2}{N}} \quad (4)$$

where $h_{fobs}(i,t)$ and $h_{fcal}(i,t)$ denote observed and calculated groundwater level obtained from Equation (1)-(3), respectively. N represents the number of time steps for selected rainfall events.

Table 3.2 Surface runoff coefficient for the groundwater recharge model

Type of ground surface	Coefficient of surface runoff, $F_{i\infty}$
Road:	
Pavement	0.70-0.90
Permeable pavement	0.30-0.40
Gravel road	0.30-0.70
Shoulder or top of slope:	
Fine soil	0.40-0.65
Corse soil	0.10-0.30
Hard rock	0.70-0.85
Soft rock	0.50-0.75
Grass plot of sand:	
Slope 0-2%	0.05-0.10
Slope 2-7%	0.10-0.15
Slope 7%	0.15-0.20
Grass plot of clay	
Slope 0-2%	0.13-0.17
Slope 2-7%	0.18-0.22
Slope 7%	0.25-0.35
Roof	1.00
Unused bare land	0.20-0.40
Athletic field	0.40-0.80
Park with vegetation	0.10-0.25
Mountain with a gentle slope	0.30
Mountain with a steep slope	0.50
A paddy field or water	0.70-0.80
Farmland	0.10-0.30

Actual evaporation of intercepted rainfall by trees

Evapotranspiration is very important factor when calculating the regional water budget. During the last decades several studies have reported on forest hydrology (e.g. Leyton et al., 1967; Johnson, 1990; Klaasen et al., 1996). Nevertheless, it is still difficult to apply these developments because necessary meteorological data is not easy to be collected. In addition, there is a problem of estimating actual evapotranspiration from potential evapotranspiration, considering interception by forest canopy, soil water

content in the unsaturated soil zone and depth of groundwater table. Hence, the way of calculating actual evapotranspiration needs to be simplified. The following section describes the simplified way.

Rainfall interception by forest canopy

Kondo et al (1992) used data from 66 regional meteorological stations in Japan to determine rainfall interception. The heat balance-bulk method was used in their study to calculate transpiration and direct evaporation of intercepted rainfall. Figure 3.4 shows the relationship between monthly precipitation and estimated monthly rainfall interception by Kondo et al. (1992), which can estimate the direct evapotranspiration from the forest canopy. The relationship made up the broken line in Figure 3.3 and the relationship describes Equation (5). This equation can be used to estimate direct evapotranspiration from monthly precipitation in Japan:

$$\frac{I_M}{r_M} = \frac{48}{r_M + 98} \qquad (5)$$

where r_M is monthly precipitation and I_M is monthly interception. During the period 1986 to 1990, the estimated mean annual interception was 305 mm/year for the mean annual precipitation of 1519 mm/year, the ratio of the interception to the precipition is approximately 20 %. According to Ogawa et al. (2001), the rainfall interception was 126.7 mm, transpiration was 101.8 mm and the throughfall was 267.0 mm for the total precipitation of 495.5 mm during the periods 15 July-15 September, 11-26 November and 1-14 December 1999. This results in that the ratio of interception equals to 25.6%. Fukushima & Suzuki (1987) also reported that the water balance calculation leaded to the ratio of the observed rainfall interception is 20% to the precipitation during the period 1971 to 1981. Furthermore, Tsukahara et al. (1992) stated that the ratio of rainfall interception ranges from 13 to 26 % in Japan. Therefore, it is reasonable to apply this method to estimate rainfall interception by forest canopy in the study area.

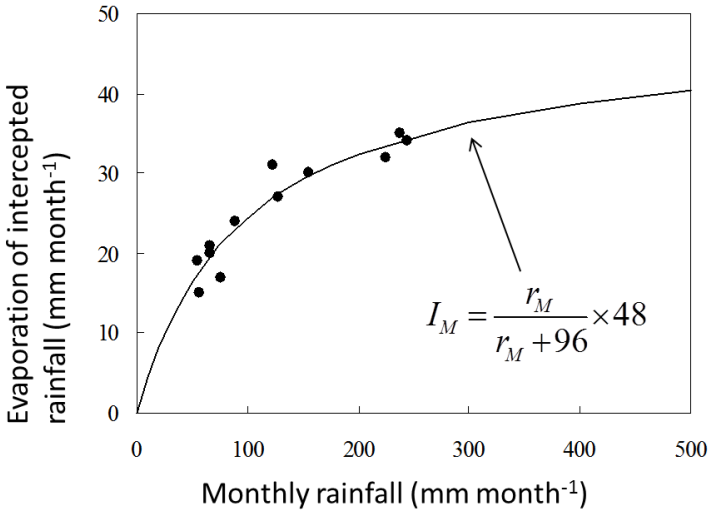

Figure 3.4 Evapotranspiration of intercepted rainfall

Calculation of hourly potential evapotranspiration

In order to use potential evapotranspiration and direct evaporation from the canopy in numerical simulations, the given monthly values need to be converted to hourly values. Kondo et al. (1992) calculated potential evapotranspiration by dividing into three subprocesses: (a) transpiration from trees, (b) evaporation from the ground surface in forest, and (c) direct evaporation from trees. They also considered three more cases depending on precipitation: (i) only transpiration from trees for days with no rain, (ii) both transpiration and direct evaporation for days with rainfall below 5 mm/day, and (iii) only direct evaporation for days with heavy rainfall (≥5 mm/day). The evaporation from the ground surface in dense forest is assumed to be negligible. The convention from monthly values to hourly values is conducted by:

- Substituting monthly rainfall r_M into equation (5) to obtain monthly direct evaporation I_M from the forest canopy.
- Calculating monthly potential evapotranspiration from the ground surface, EVT_g (mm/month) from Equation (6);

$$EVT_g = EVT_{pTH} - I_M \qquad (6)$$

  where EVT_{pTH} is monthly potential evapotranspiration calculated by the Thornthwaite method.
- Counting the number of no rain days, n_a, and days with little rainfall, n_b, to calculate the hourly potential evapotranspiration EVT_{gh} (mm/hour) from Equation (7):

$$\mathrm{EVT}_{gh} = \frac{EVT_g}{12n_a + 6n_b} \quad (7)$$

Water uptake from groundwater through the unsaturated zone

Capillary water flows upward and water is taken by tree roots from the groundwater table when H_g, the distance between ground surface and groundwater table, is smaller than H_g^*. Since groundwater table is shallower than H_g^* along rivers and springs, the water uptake from groundwater would be significant in the areas. Whereas the effect takes place where groundwater table is shallow, it does not take place where groundwater table is deeper than H_g^*.

In the areas where groundwater is shallower than H_g^* additional evapotranspiration denoted by $EVT_2(t)$, occurs after the groundwater in the tank is exhausted. The procedure of the calculation of $EVT_1(t)$ is summarized below. It is assumed that additional evapotranspiration $EVT_1(t)$ takes place from 06:00 and 18:00 for days with no rain, and from 09:00 to 18:00 for days with rainfall below 5 mm/day (Kondo et al., 1992).

If the water in the tank is not exhausted after Δt, $EVT_1(t)$ is calculated as;

$$EVT_1(t) = EVT_{gh} \quad (8)$$

If the water in the tank is exhausted after Δt, $EVT_1(t)$ is;

$$EVT_1(t) = \frac{h_w(t)}{\Delta t} + \{1 - F(r)\}r(t) - q_w(t) \quad (9)$$

As seen in Equation (9), the evapotranspiration lasts until the water in the tank becomes empty.

For the other period, $EVT_1(t)$ is described as;

$$EVT_1(t) = 0 \quad (10)$$

The procedure of the calculation of $EVT_2(t)$ is summarized below.

If the groundwater table is shallower than H_g^*, $EVT_2(t)$ is;

$$EVT_2(t) = EVT_{gh} - EVT_1(t) \quad (11)$$

If the groundwater table is deeper than H_g^*, $EVT_2(t)$ is calculated as;

$$EVT_2(t) = 0 \quad (12)$$

The conditions presented above depend on the numerical result of groundwater table h_f. The calculation is shown in Equation (13) and (14) which are presented in the next part. Since H_g^* can be estimated spatially, catchment distribution of actual evapotranspiration is calculated in the model simulation. According to Anderson & Woessner (1992), H_g^* ranges from 1.8 m to 2.4 m, which is determined by the depth of plant roots.

Quasi three-dimensional two-phase groundwater flow equation

The quasi three-dimensional salt- and freshwater two phase groundwater flow equation is applied to calculate groundwater table. The presented groundwater recharge model is linked to Equation (13) which is freshwater flow equation. Groundwater table can be estimated by taking into account groundwater pumping, groundwater recharge and evaporation from groundwater table. Equation (14) represents the salt groundwater flow which is a function of porosity, impermeable base elevation and saltwater velocity. This equation can calculate fresh-saltwater interface but the result is not used for the numerical simulation in this study.

The basic equations describing fresh and salt groundwater flow respectively are:

$$n_e \frac{\partial(h_f - h_s)}{\partial t} = -\frac{\partial\{(h_f - h_s)\cdot u_f\}}{\partial x} - \frac{\partial\{(h_f - h_s)\cdot v_f\}}{\partial y} - \sum_m Q_m(x,y,t)\delta(x - x_m)\delta(y - y_m) + q_w(x,y,t) - EVT_2(x,y,t) \quad (13)$$

$$n_e \frac{\partial h_s}{\partial t} = -\frac{\partial[\{h_s - b(x,y)\}\cdot u_s]}{\partial x} - \frac{\partial[\{h_s - b(x,y)\}\cdot v_s]}{\partial y} \quad (14)$$

where h_f, h_s are fresh groundwater elevation and fresh-saltwater interface elevation, respectively. b(x, y) is the impermeable base elevation taken from the reference level. u_f, v_f, u_s and v_s are the freshwater and saltwater velocities in x and y direction. $Q_m(x, y, t)$ is the groundwater pumping rate at location (x_m, y_m) at time t. The delta functions $\delta(x-x_m)$ and $\delta(y-y_m)$ denote the position of the pumping well. $EVT_2(x, y, z)$ is evapotranspiration from groundwater table. $q_w(x, y, t)$ represents the groundwater recharge that are obtained from Equation (1) and (2). To solve the partial differential equations, this model employs the finite difference method.

3.2.2. Three dimensional density dependent solute transport model

Darcy's low

The Darcy's low can be described as follows;

$$u = -k_x(h)\frac{\partial h}{\partial x} \quad (15\text{-a})$$

$$v = -k_y(h)\frac{\partial h}{\partial y} \quad (15\text{-b})$$

$$w = -k_z(h)\left(\frac{\partial h}{\partial z} + \frac{\rho}{\rho_f}\right) \quad (15\text{-c})$$

where u, v and w are the Darcy's velocities in x, y and z directions, respectively. $k_x(h)$, $k_y(h)$ and $k_z(h)$ are the hydraulic conductivities in x, y and z directions, respectively. h is the hydraulic pressure head. P is the domain water velocity and ρ_f is the freshwater density.

Three dimensional saturated-unsaturated flow equation

The continuity equation takes into account the mass balance of water inside an infinitesimal control volume with dimensions Δx, Δy and Δz in the three dimensional space (Figure 3.5). If there is no sink/source inside the control volume, the continuity equation will be as bellow:

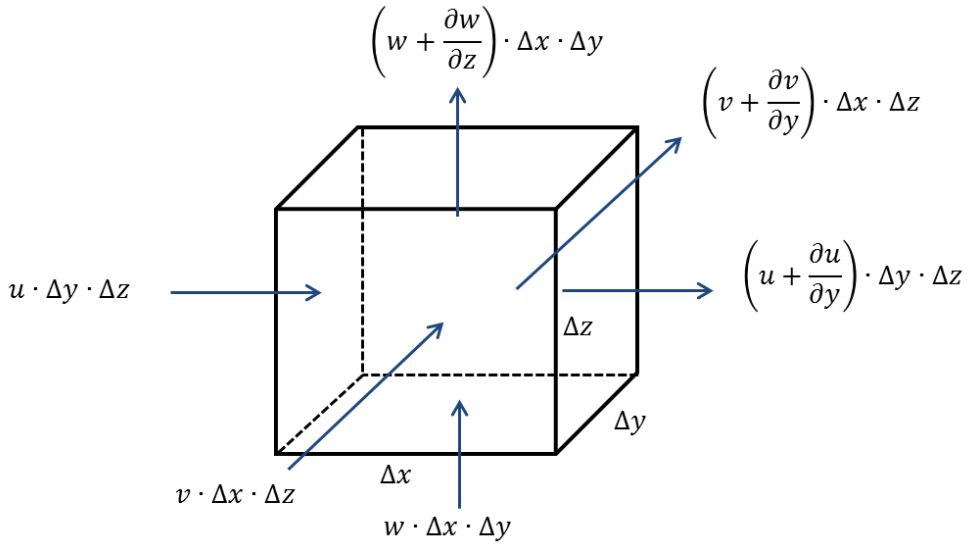

Figure 3.5 Control Volume

$$\begin{aligned}\Delta v &= \Delta x \cdot \Delta y \cdot \Delta z \\ &= \frac{\partial(\theta \cdot \Delta x \cdot \Delta y \cdot \Delta z)}{\partial t} \\ &= u \cdot \Delta z \cdot \Delta y + v \cdot \Delta x \cdot \Delta w + w \cdot \Delta x \cdot \Delta y \\ &\quad - \left[\left(u + \frac{\partial u}{\partial x} \cdot \Delta x\right) \cdot \Delta z \cdot \Delta y + \left(v + \frac{\partial v}{\partial y} \cdot \Delta y\right) \cdot \Delta x \right. \\ &\quad \left. \cdot \Delta w + \left(w + \frac{\partial w}{\partial z} \cdot \Delta z\right) \cdot \Delta x \cdot \Delta y\right]\end{aligned} \tag{16}$$

where θ is the volumetric water content. Above expression can be reduced to:

$$\frac{\partial(\theta \cdot \Delta x \cdot \Delta y \cdot \Delta z)}{\partial t} = -\left(\frac{\partial u}{\partial x} + \frac{\partial v}{\partial y} + \frac{\partial w}{\partial z}\right) \Delta x \cdot \Delta y \cdot \Delta w \tag{17}$$

It is written as;

$$\frac{\partial \theta}{\partial t} = -\left(\frac{\partial u}{\partial x} + \frac{\partial v}{\partial y} + \frac{\partial w}{\partial z}\right) \tag{18}$$

Above can be written as

$$\frac{\partial \theta}{\partial t} = \frac{\partial \theta}{\partial h} \cdot \frac{\partial h}{\partial t} \tag{19}$$

If specific moisture capacity,

$$C_w = \frac{\partial \theta}{\partial h} \tag{20}$$

Then the complete equation for both saturated and unsaturated flow can be written in terms of the hydraulic pressure head, h:

$$(C_w + \alpha S_s) \cdot \frac{\partial h}{\partial t} = -\left(\frac{\partial u}{\partial x} + \frac{\partial v}{\partial y} + \frac{\partial w}{\partial z}\right) \tag{21}$$

where t is time, S_S is the specific storage coefficient, C_w is the specific moisture capacity, α is a dummy which takes 0 in the unsaturated condition and 1 in the saturated condition.

van Genuchten formula for unsaturated zone

In the density dependent solute transport model, the pressure head is solved for both saturated and unsaturated zones simultaneously. For the calculation of the unsaturated zone flow the unsaturated flow parameters need to be considered. Therefore, it is necessary to define the relationship between the negative pressure head, h and the unsaturated flow parameters such as the volumetric water vcontent θ, the ratio of hydraulic conductivity k_r and the unsaturated hydraulic conductivity k_r and the specific moisture capacity C_w. van Genuchten (1980) explained the deviation of unsaturated flow parameters as below.

$$S_0 = \frac{\theta - \theta_r}{\theta_s - \theta_s} \tag{22}$$

$$S_e = \left[\frac{1}{1 + (\alpha|h|)^n}\right]^m \tag{23}$$

$$k_r = S_0^{1/2}\left\{1 - \left(1 - S_e^{1/m}\right)^m\right\}^m \tag{24}$$

$$C_w = \frac{\alpha \cdot m(\theta_s - \theta) S_e^{1/m}(1 - S_e^{1/m})^m}{1 - m} \tag{25}$$

where Θ_r is the residual water content, Θ_s is the saturated water content and α, m and n are the coefficient of the van Genuchten formula.

Solute transport equation for advection and dispersion

In three dimensional transient groundwater flow system, the partial differential equation can be written as;

$$\frac{\partial C}{\partial t} = \frac{\partial}{\partial x}\left(D_{xx}\frac{\partial C}{\partial x} + D_{xy}\frac{\partial C}{\partial y} + D_{xz}\frac{\partial C}{\partial z}\right) + \frac{\partial}{\partial y}\left(D_{yx}\frac{\partial C}{\partial x} + D_{yy}\frac{\partial C}{\partial y} + D_{yz}\frac{\partial C}{\partial z}\right) + \frac{\partial}{\partial z}\left(D_{zx}\frac{\partial C}{\partial x} + D_{zy}\frac{\partial C}{\partial y} + D_{zz}\frac{\partial C}{\partial z}\right) - \left(u'\frac{\partial C}{\partial x} + v'\frac{\partial C}{\partial y} + w'\frac{\partial C}{\partial z}\right) \quad (26)$$

where C is the solute concentration, u', v' and w' are real pore velocities in x, y and z direction, respectively. u', v' and w' are described as ;

$$u' = \frac{u}{\theta} \quad (27\text{-a})$$

$$v' = \frac{v}{\theta} \quad (27\text{-b})$$

$$w' = \frac{w}{\theta} \quad (27\text{-c})$$

D_{xx}, D_{yy}, D_{zz}, D_{xy}, D_{xz}, D_{yz}, D_{yx}, D_{yz}, D_{zx} and D_{zy} are dispersion coefficients which are calculated as;

$$D_{xx} = \alpha_L\frac{u'^2}{|V|} + \alpha_T\frac{v'^2}{|V|} + \alpha_T\frac{w^2}{|V|} + \tau \cdot D_M \quad (28\text{-a})$$

$$D_{yy} = \alpha_T\frac{u'^2}{|V|} + \alpha_L\frac{v'^2}{|V|} + \alpha_T\frac{w^2}{|V|} + \tau \cdot D_M \quad (28\text{-b})$$

$$D_{zz} = \alpha_T\frac{u'^2}{|V|} + \alpha_T\frac{v'^2}{|V|} + \alpha_L\frac{w'^2}{|V|} + \tau \cdot D_M \quad (28\text{-c})$$

$$D_{xy} = D_{yx} = (\alpha_L - \alpha_T)\frac{u' \cdot v'}{|V|} \quad (28\text{-d})$$

$$D_{xz} = D_{zx} = (\alpha_L - \alpha_T)\frac{u' \cdot w'}{|V|} \quad (28\text{-e})$$

$$D_{yz} = D_{zy} = (\alpha_L - \alpha_T)\frac{w' \cdot v'}{|V|} \quad (28\text{-f})$$

(Sato et al., 2003)

where D_{xx}, D_{yy} and D_{zz} are the principal components of the dispersion tensor while D_{xy}, D_{yx}, D_{xz}, D_{zx}, D_{yz} and D_{zy} are the cross terms of the dispersion tensor. When the velocity vector is aligned with one of the coordinate axes, all the cross terms become zero.

α_L and α_T are the longitudinal dispersion length and the transverse dispersion length, respectively. D_M is the molecular diffusion coefficient, and τ is the tortuosity.

V is the magnitude of the velocity vector which is written as below.

$$|V| = \sqrt{(u'^2 + v'^2 + w'^2)} \quad (29)$$

Equation of state

Equations (21) and (26) are coupled in the variable-density groundwater flow system. Fluid density is a function of solute concentration and the solute transport is dependent on the flow fluid. The relationship between fluid density and solute concentration is represented by an equation of state, which can be approximated with the following literalized form. The presented equation of state does not include the dependence of fluid density on temperature or pressure, and thus Equation (30) is valid for isothermal systems with an incompressible fluid. For deep aquifer systems and for aquifers with large temperature variations, an equation based on pressure, temperature, and solute concentration is required. Diersch and Kolditz (2002) provide a summary of more rigorous forms of equations of states. For the numerical simulations of present studies following simplified equation of state is used.

$$C = \left[\left(\frac{\rho - \rho_f}{\rho_s - \rho_f}\right) \times 100\right] \quad (30)$$

where C is the salt concentration of water in the flow domain; C=100% represents the seawater and C=0% represents the freshwater. ρ_f and ρ_s are the density of seawater and freshwater, respectively. During the numerical simulation, changes in solute transportation by advection-dispersion and molecular diffusion affect the density and thus the groundwater flow.

Finite difference method

The finite difference method was the first method used for the systematic numerical solution of partial differential equation. In general, the method consists of an approximation of partial derivatives by algebraic expressions involving the values of the dependent variable at a limited number of selected points. As the result of the approximation, the partial differential equation describing the problem is replaced by a finite number of algebraic equations, written in terms of the values dependent variable at the selected points. The equations are linear if the original partial differential equations are linear. The values at the selected points become unknown, rather than the continuous spatial distribution of the dependent variable,

Finite difference approximation

The finite difference approximations are derived from the fundamental definition of derivative Taylor series expansion of a function f(x). When a

function f(x) and its derivatives are single valued, finite and continuous function of x, then by Taylor's series:

$$f(x+\Delta x) = f(x) + \frac{df(x)}{dx}\cdot\Delta x + \frac{1}{2}\cdot\frac{d^2f(x)}{dx^2}\cdot\Delta x^2 + \frac{1}{6}\cdot\frac{d^3f(x)}{dx^3}\cdot\Delta x^3 + \cdots + \frac{1}{n}\cdot\frac{d^nf(x)}{dx^n}\cdot\Delta x^n \quad (31)$$

$$f(x-\Delta x) = f(x) - \frac{df(x)}{dx}\cdot\Delta x + \frac{1}{2}\cdot\frac{d^2f(x)}{dx^2}\cdot\Delta x^2 - \frac{1}{6}\cdot\frac{d^3f(x)}{dx^3}\cdot\Delta x^3 + \cdots + \frac{1}{n}\cdot\frac{d^nf(x)}{dx^n}\cdot(-\Delta x)^n \quad (32)$$

Addition and subtraction of above expansions give Equations (33) and (34), respectively as follows:

$$\frac{d^2f(x)}{dx^2} = \frac{f(x+\Delta x) - 2f(x) + f(x-\Delta x)}{(\Delta x)^2} + O\{(\Delta x)^n\} \quad (33)$$

$$\frac{df(x)}{dx} = \frac{f(x+\Delta x) - f(x-\Delta x)}{2\Delta x} + O\{(\Delta x)^n\} \quad (34)$$

where $O\{(\Delta x)^n\}$ is the terms containing the second and higher orders of Δx.

Approximation of Equations (31) and (32) after ignoring the higher derivative terms result in a truncation error of the order of $(\Delta x)^2$. Equations (31) and (32) can be approximated by the first derivative with a truncation error of order Δx, respectively, as follows:

$$\frac{df(x)}{dx} = \frac{f(x+\Delta x) - f(x)}{\Delta x} + O\{(\Delta x)^2\} \quad (35)$$

$$\frac{df(x)}{dx} = \frac{f(x) - f(x-\Delta x)}{\Delta x} + O\{(\Delta x)^2\} \quad (36)$$

The finite difference approximation given by Equations (34), (35) and (36) in terms of truncation error are called the central difference, the forward difference, and the backward difference formulas

Method of Characteristic

The method of solving the advection component of the solute transport equation by finite difference method is often subject to two problems; numerical dispersion and artificial oscillation.

Numerical dispersion is a problem which introduces truncation errors, leading to the smearing of concentration fronts which should be a sharp front (Figure 3.6).

Artificial oscillations often occur in the solution of the solute transport equation which results from overshoot and undershoot of the concentrations (Figure 3.7).

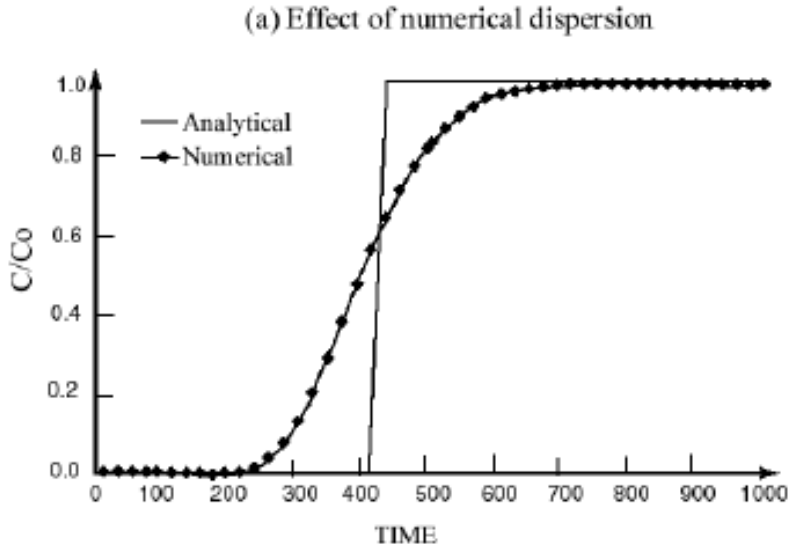

Figure 3.6 Effect of numerical dispersion (Weixing et al., 2002)

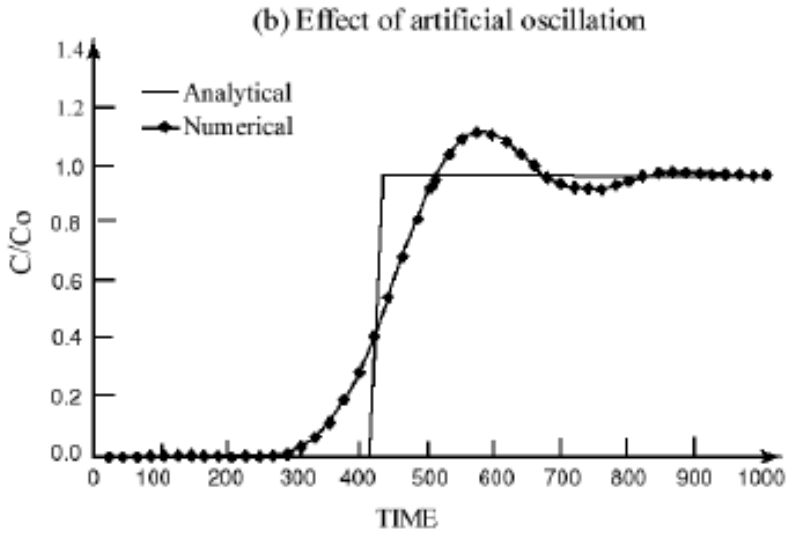

Figure 3.7 Effect of artificial oscillation (Weixing et al., 2002)

The method of characteristics employs a conventional particle tracking technique. As the initial step of the technique, a group of moving particles is distributed in the flow field either randomly or with a fixed pattern. A

concentration and position in the Cartesian coordinate system are associated with each of the particles. In each time increment the particles are allowed to move with the flow and are tracked. At the end of each time increment, the average concentration at cell v due to advection alone over the time increment, i.e. $C_V^{n^*}$, is evaluated from the concentration of moving particles which are located within that cell (Figure 3.8).

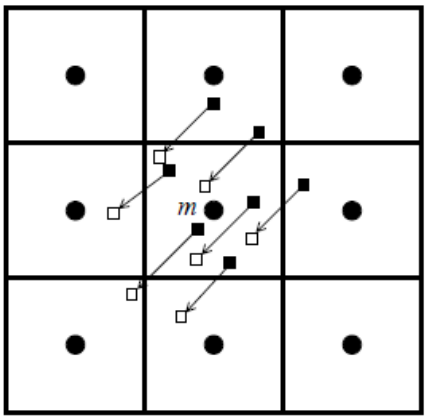

Fig. 3.5.
Illustration of the method of characteristics (MOC). A set of moving particles are tracked forward during each time period. An intermediate concentration for cell *m*, equal to the weighted average of the concentrations of all particles in the cell, is computed. This intermediate concentration accounts for the effect of advection alone during a time increment Δt, and is used to calculate changes in concentration due to dispersion and other processes over that time increment.

Figure 3.8 Illustration of particle tracking method (Weixing et al., 2002)

The above mentioned is the procedure of method of characteristic in solving advection term of solute transport equation. The below explained is the numerical implementation of the method of characteristic and finite difference method in the solute transport equation.
The Eulerian formation of solute transport equation is:

$$\frac{\partial \mathrm{C}}{\partial \mathrm{t}} = \frac{1}{\theta}\left(\theta D_{ij}\frac{\partial \mathrm{C}}{\partial \mathrm{x}_i}\right) - \frac{1}{\theta}u_i\frac{\partial \mathrm{C}}{\partial \mathrm{x}_i} \qquad (37)$$

In Equation (37), $\frac{\partial \mathrm{C}}{\partial \mathrm{t}}$ represents the rate of change in solute concentration at a fixed point in space. The dispersion part of the Equation (37) can also be expressed in Lagrangian form as;

$$\frac{\mathrm{dC}}{\mathrm{dt}} = \frac{1}{\theta}\left(\theta D_{ij}\frac{\partial \mathrm{C}}{\partial \mathrm{x}_i}\right) \qquad (38)$$

where $\frac{\mathrm{dC}}{\mathrm{dt}} = \frac{\partial \mathrm{C}}{\partial \mathrm{t}} + \frac{1}{\theta}u_i\frac{\partial \mathrm{C}}{\partial \mathrm{x}_i}$ represents the rate of change in solute concentration along the path line of a contaminant particle or a characteristic curve of the velocity field. By introducing the finite difference algorithm, the substantial derivative in Equation (38) can be approximataed as;

$$\frac{\mathrm{dC}}{\mathrm{dt}} = \frac{C_i^{t+1} - C_i^t}{\Delta t} \tag{39}$$

Equation (39) can be rewritten as;

$$C_i^{t+1} = C_i^{n*} + \Delta t \times RHS \tag{40}$$

where C_i^{t+1} is the solute concentration at node (i) at new time level n+1. C_i^{t*} is the solute concentration at node (i) at new time level t+1 due to advection alone, also referred as intermediate time level t*. Δt is the time increment between old time level t and new time level t+1. RHS is the right hand side of Equation which is solved by finite difference method.

Now to find the value of advection term C_i^{t*} the method of characteristic is applied.

A set of particles is distributed and allowed to move with the flow as explained above. After the time has increased from time level t to t+1, i.e. after Δt time increment the average particle concentration related to the particular node is calculated.

If a simple arithmetic averaging is used, the average concentration can be expressed as:

$$C_v^{n*} = \frac{1}{NP_v} \sum_{i=1}^{NPi} C_i^n \qquad \text{If} \quad NP_m > 0 \tag{41}$$

where NP_m is the number of particles within cell v. C_v^n is the concentration of the i^{th} particle at the old time level (t).

After calculating the C_v^{n*} for all cells, a weighted concetration, $C_v^{n\wedge}$ is calculated based on C_v^{n*} and the concentration of old time interval C_v^n;

$$C_v^{n\wedge} = \omega C_v^{n*} + (1 - \omega) C_v^n \tag{42}$$

where ω is a weighting factor 0.5 and 1.

$C_v^{n\wedge}$ is then used to calculate the second term in the solute transport equation, or the changes in concentration due to dispersion. Generally the second term is solved by finite difference method. If the explicit finite difference method is used;

$$\Delta C_v^{n+1} = \Delta t \times RHS(C_v^{n\wedge}) \tag{43}$$

The concentration for cell v at new time interval (t+1), C_v^{n+1} is;

$$\Delta C_v^{n+1} = C_v^{n*} + \Delta C_v^{n+1} \tag{44}$$

The concentrations of all moving particles are also updated to reflect the change due to dispersion. This completes the calculation of one transport step for the method of characteristic.

Successive over relaxation method (SOR)

The successive over- relxation method (SOR) is derived by applring extrapolation to the Gauss-Seidel method. This extrapolation takes the form of a weighted average between the previous iterate and the computed Gauss-Seidel iterate successively for each component:

$$x_i^{(n)} = \omega \bar{x}_i^n + (1-\omega) x_i^{n-1} \quad (45)$$

where $\bar{x}$ denotes a Gauss-Seidel iterate, and ω is the extrapolation factor. The idea is to choose a value for ω that will accelerate the rate of convergence of the iterates to the solution. When ω=1 is selected the iteration method is called Gauss-Seidel iteration, when ω=0.5 is selected the iteration method is called Crank-Nicholson scheme (Bear et al., 1997). In the numerical simulation of this thesis the value which was used forω=0.5.

3.4. Numerical model

The simulation model domain in the recharge model simulation is larger than the solute transport model simulation to consider a large number of factors. In the recharge model simulation, the simulation domain is divided with a grid length of 50 m in the x direction and 25 m in the y direction. On the other hand, the model domain for the solute transport model is divided with a grid length 9 m in the x direction, 6.5 m in the y direction and 2 m in the z direction. Hence, the results from the recharge model simulation are linearly interpolated to use as input data for the solute transport model. The time increment is 3600 seconds. The grid sizes and the time increment for the both simulation are determined considering simulation time.

Parameters for the simulations have to be determined by available information. For the recharge model simulation, the parameters that Tsutsumi et al. (2004) estimated are used. The hydro-geological parameters for the solute transport simulation are determined by boring surveys and previous study (Perara, 2011). The used parameters are listed in Table 3.3.

Table 3.3 Hydrological parameters for the density dependent solute transport model

Parameter	Value
Hydraulic conductivity for bed rock	1.0×10^{-11} (m/s)
Hydraulic conductivity for confined layer	6.6×10^{-7} (m/s)
Hydraulic conductivity for aquifer	4.6×10^{-4} (m/s)
Longitudinal dispersion length	3.6 (m)
Transverse dispersion length	0.36 (m)
Molecular diffusion	1.0×10^{-9} (m^2/s)
Specific storage coefficient	6.3×10^{-6} (m^{-1})
Freshwater density	1000.0 (kg/m^3)
Seawater density	1025.0 (kg/m^3)
Saturated water content	0.3
Residual water content	0.108

The finite difference method is used to solve the partial differential equation of flow (Continuity equation and Darcy's equation) and the diffusion component of the three dimensional density dependent solute transport equation. However, in order to avoid the problems which are mentioned above, the method of characteristic (MOC) is used to solve advection component of the solute transport equation. For the application of the method of characteristic 8 particles are distributed uniformly for each grid at the beginning as shown in Figure 3.9. Initially, 1.05 million particles are assigned to the model. The number of particles is determined considering the simulation time.

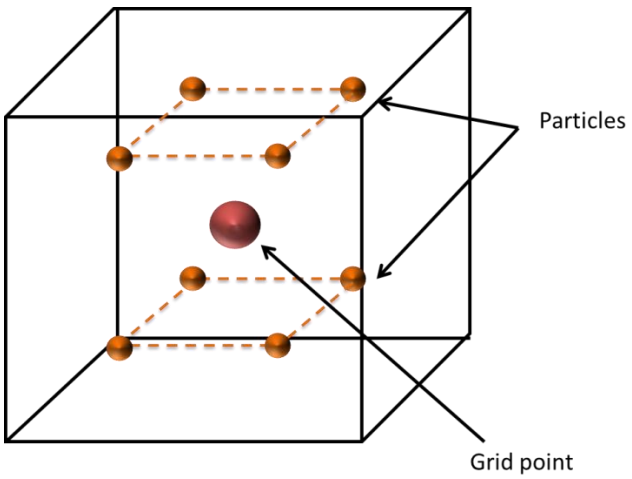

Figure 3.9 Initial displacements of particles for MOC

For the initial condition the model boundary needs to be defined. Figure 3.10 and Table 3.4 show the defined model boundaries. The boundary conditions are obtained from Dirchlet boundary condition, Neumann boundary conditions and Cauchy boundary conditions (Weixing et al., 2002). The model consists of 6 boundaries; top surface (EFGH), bottom surface (ABCD), seaside boundary (HDCG), mountainside boundary (EABF), right side boundary (EADH) and left side boundary (FBCG).

For the top surface and bottom surface a flux boundary due to groundwater recharge and a zero flow boundary are assigned, respectively. The other boundaries are assigned with timely dependent pressure head boundaries which vary with water table height of boundaries.

As described in the previous par, these water table heights of boundaries are estimated through groundwater recharge model.

The concentrations at the boundaries are defined as; zero concentration at the mountainside boundary (EABF) and 100% concentration at the seaside boundary (HDCG). For the 4 vertical boundaries the concentration gradient is zero.

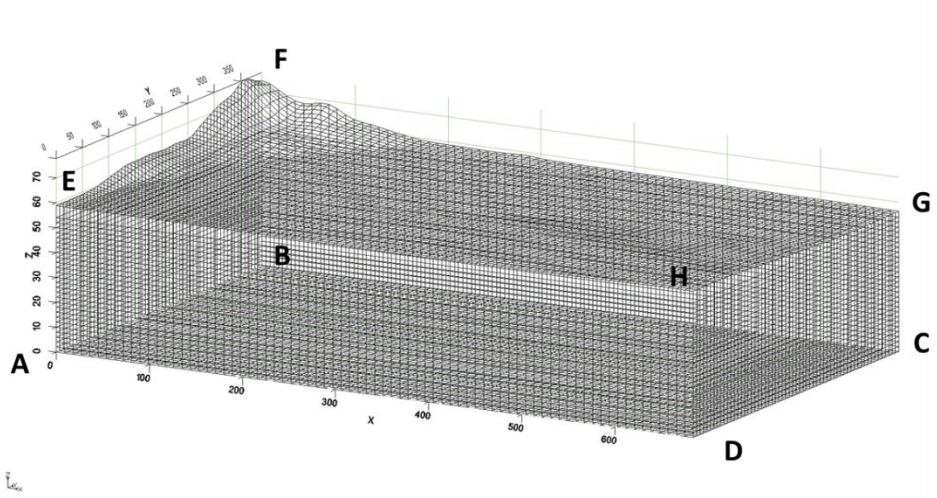

Figure 3.10 Boundaries of the model region

Table 3.4 Boundary conditions for pressure head and concentration

Boundary	Pressure head	Concentration
EADH	$\mathrm{h}(t) = H(t) - y$	$\frac{\partial C}{\partial \mathrm{y}} = 0.0$
FBCG	$\mathrm{h}(t) = H(t) - y$	$\frac{\partial C}{\partial \mathrm{y}} = 0.0$
EABF	$\mathrm{h}(t) = H(t) - y$	$C = 0.0\%$
HDCG	$\mathrm{h}(t) = (H_{sea} - y) \cdot \frac{\rho}{\rho_f}$	$C = 100\%$
ABCD	$-k(h)\left[\frac{\partial h}{\partial z} + \frac{\rho}{\rho_f}\right] = 0$	$\frac{\partial C}{\partial z} = 0.0$
EFGH	$-k(h)\left[\frac{\partial h}{\partial z} + \frac{\rho}{\rho_f}\right] = -\mathrm{Re(t)}$	$\frac{\partial C}{\partial z} = 0.0$

The numerical model is coded by FORTRAN programming language. The flow of the main simulation of the solute transport model is illustrated in Figure 3.11.

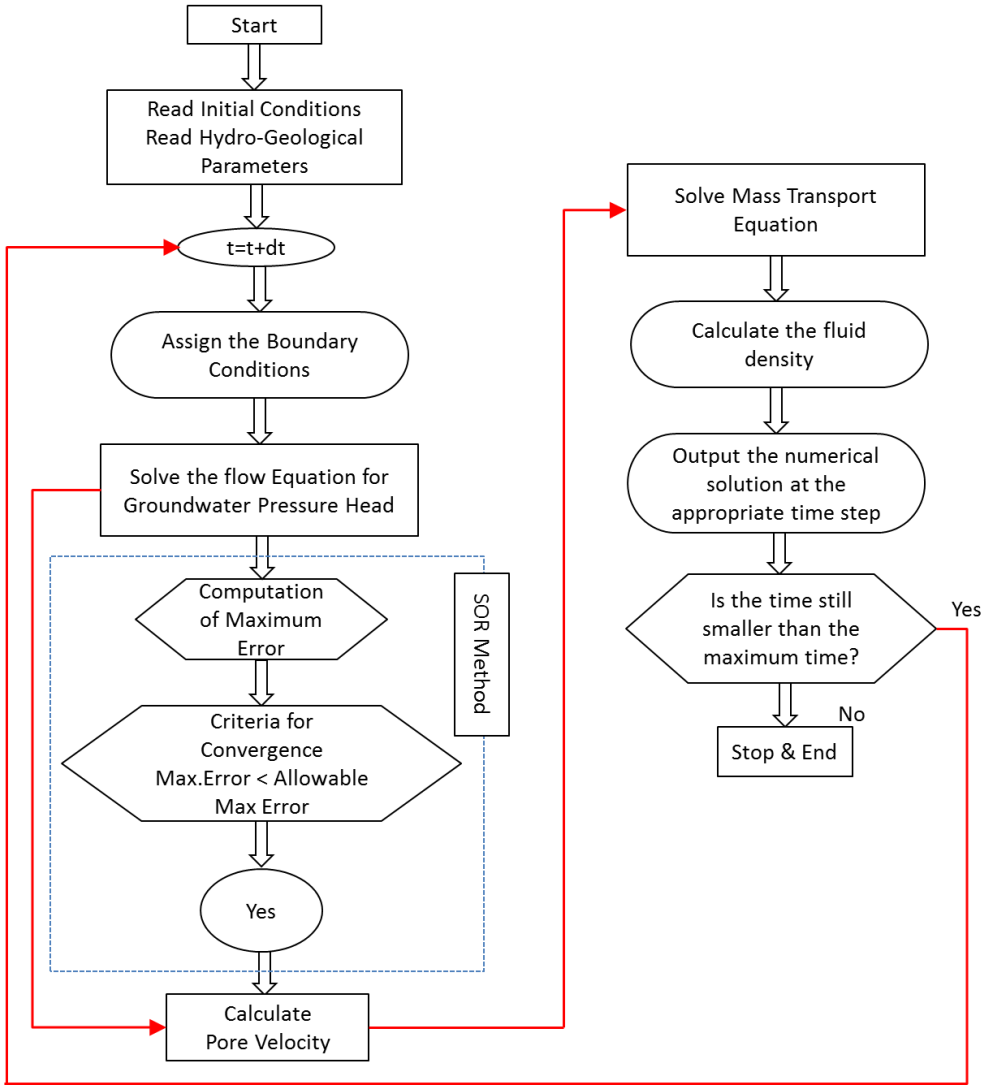

Figure 3.11 Flow chart of three dimensional solute transport model simulation

4. Numerical results

4.1. Validity of the model simulation

The validity of the model simulation is discussed in this part. The calculated water level and electric conductivity values from the validation period are evaluated by comparing with the observed values. Figure 4.1 illustrates the comparison of the observed and the calculated groundwater level at the observation well WL5 from 2005 to 2010. The fluctuation of water level can be explained as a result of the groundwater pumping and groundwater recharge. The result shows that the model responds well with the groundwater pumping and recharge, which leads to a reasonable correlation with the observed groundwater level.

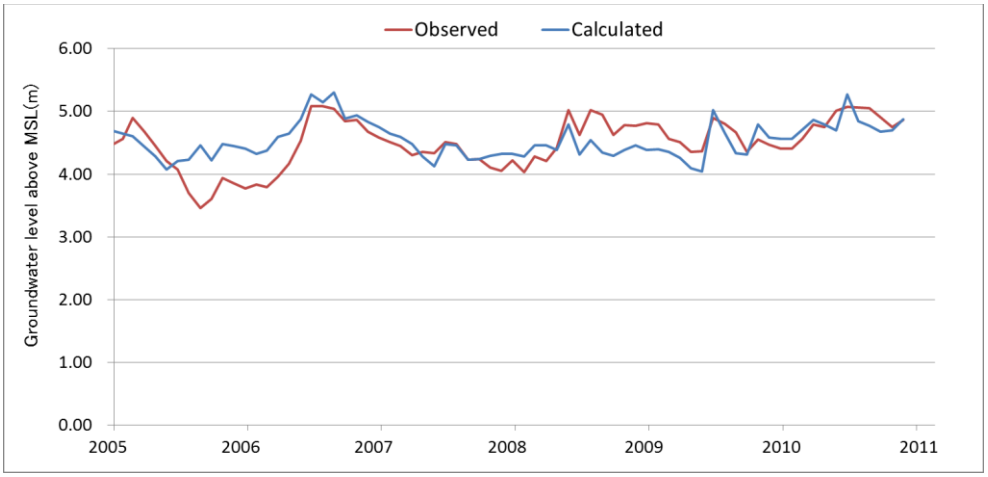

Figure 4.1 Observed and calculated water level at the observation well WL5 from 2005 to 2010

Figure 4.2 shows the comparisons of the observed and the calculated electric conductivities with depth at the EC observation well B7-4 for February and June of 2008, 2009 and 2010. The observed fresh-saltwater interface is lower than the calculated interface for February of 2010. This difference is caused by the irregular groundwater pumping rates. However, the calculated and observed electric conductivities show reasonable correlation in the other periods when some amount of groundwater is discharged.

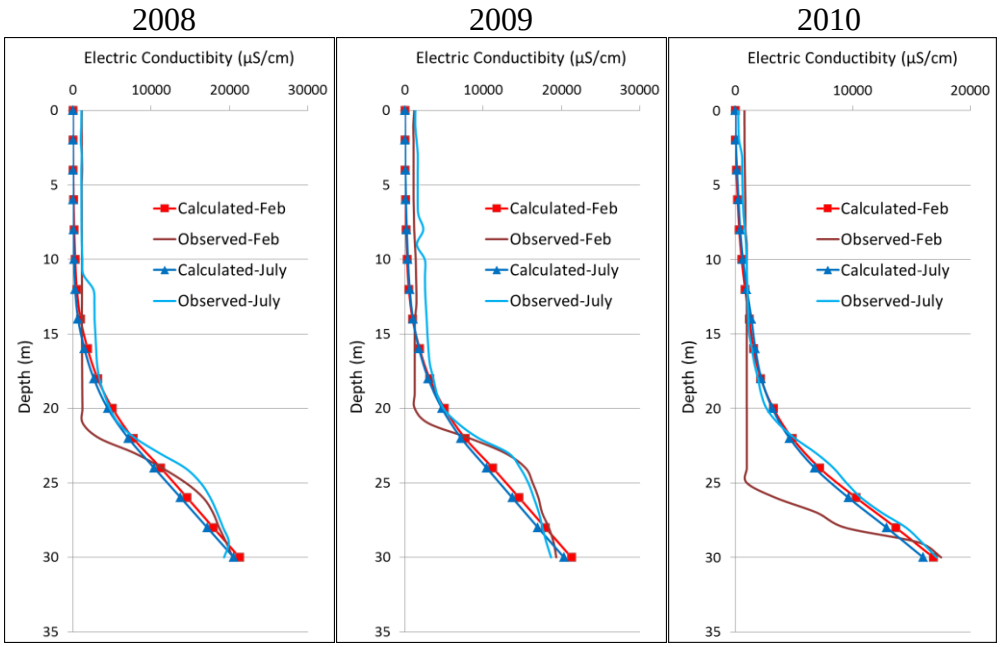

Figure 4.2 Comparisons of the observed and calculated electric conductivities with depth at the borehole B7-4

4.2. Numerical results in the three cases

Figure 4.3 and 4.4 show the ratios of groundwater recharge, surface runoff and evapotranspiration to precipitation for Case 1 and Case 2 in the estimation period, respectively. Note that the ratios in Case 3 are same as those in Case 1 since groundwater pumping does not affect the three components. The ratios of groundwater recharge, surface runoff and evapotranspiration in Case 1 are 30-40 %, 30-40 % and 30 %, respectively. On the other hand, in Case 2 the ratio of groundwater recharge decreases with time while the ratio of the surface runoff increases. The recharge ratio ranges from 20 to 30 % with the impervious surface rate of 44.6% for the period 2011-2015, 10 to 15 % with that of 77.4 % for the period 2016-2020 and nearly 0 % with that of 100% for the period 2021-2030.

Moreover, the evapotranspiration decreases with the increase in impervious surface. This is because the transpiration decreases with less vegetation and the evapotranspiration from unsaturated zones and groundwater table is intercepted by the impervious surfaces.

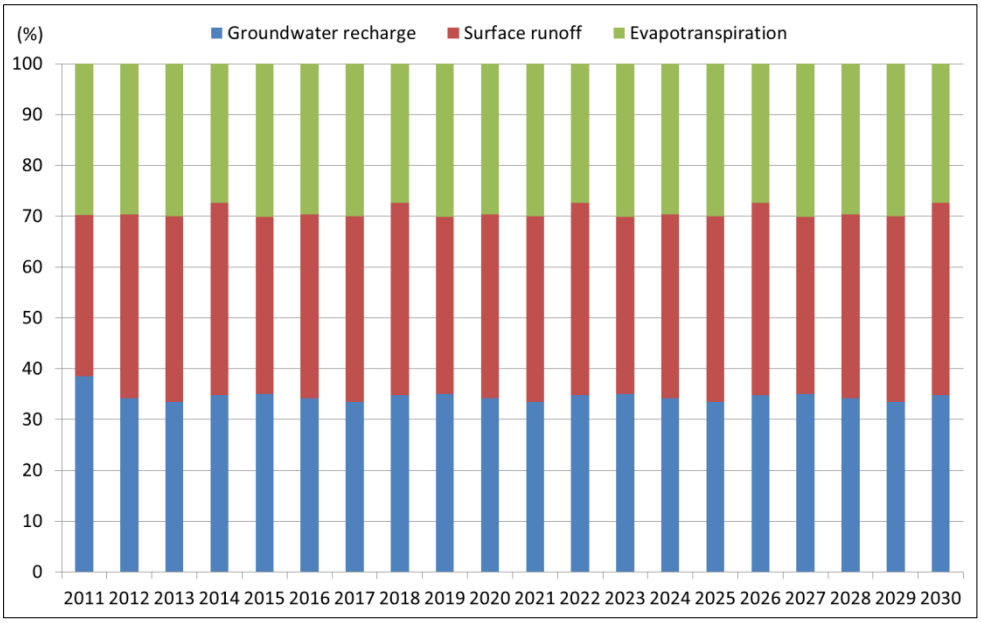

Figure 4.3 Ratios of groundwater recharge, surface runoff and evapotranspiration in Case 1 from 2011 to 2030

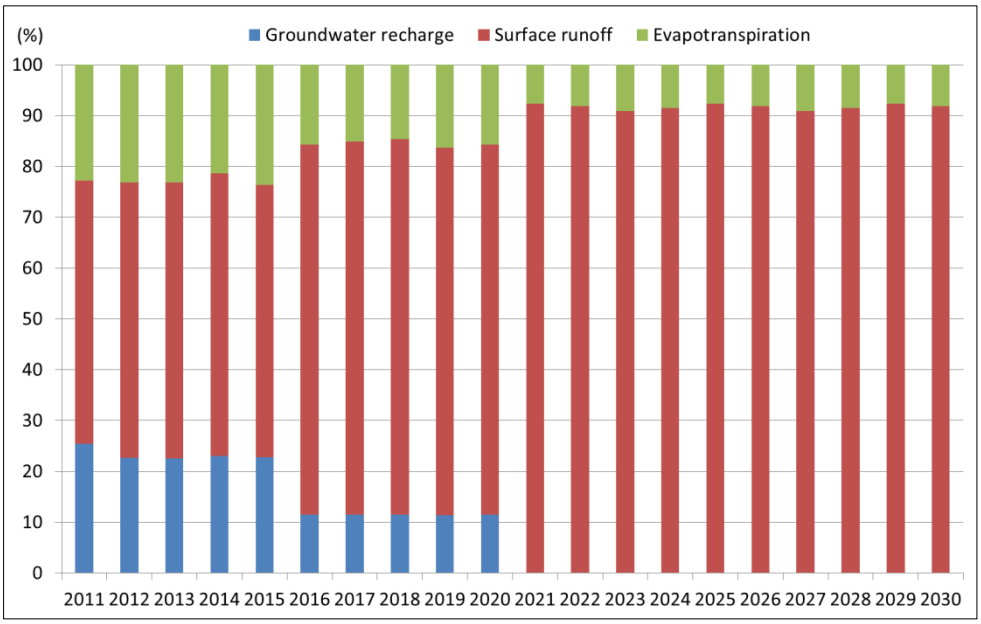

Figure 4.4 Ratios of groundwater recharge, surface runoff and evapotranspiration in Case 2 from 2011 to 2030

Figure 4.5, 4.6 and 4.7 describe the cross-section views of pressure head along the pumping well P3 for 2011, 2020 and 2030, respectively. These figures show the drawdown around the well due to the pumping. The

drawdown is larger in Case 3 than Case 1 and 2 since the drawdown is proportional to the pumping rate.

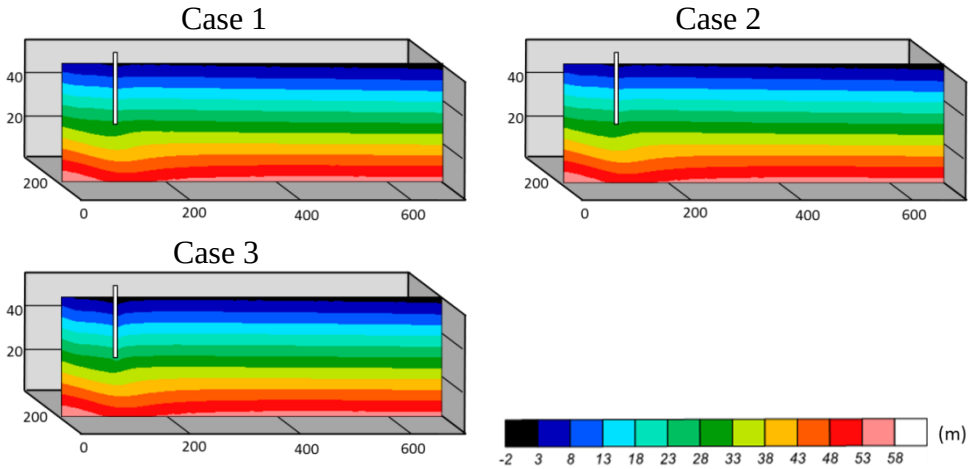

Figure 4.5 Cross-section views of pressure head in the three cases for 2011

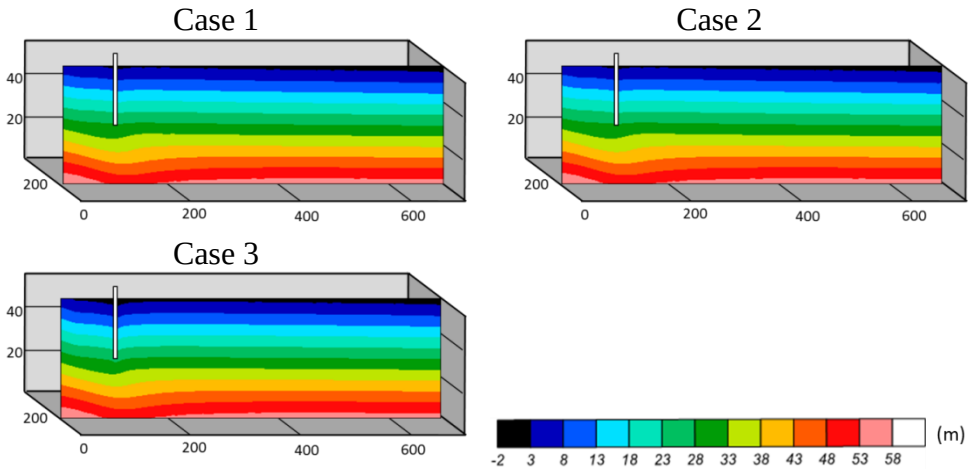

Figure 4.6 Cross-section views of pressure head in the three Cases for 2020

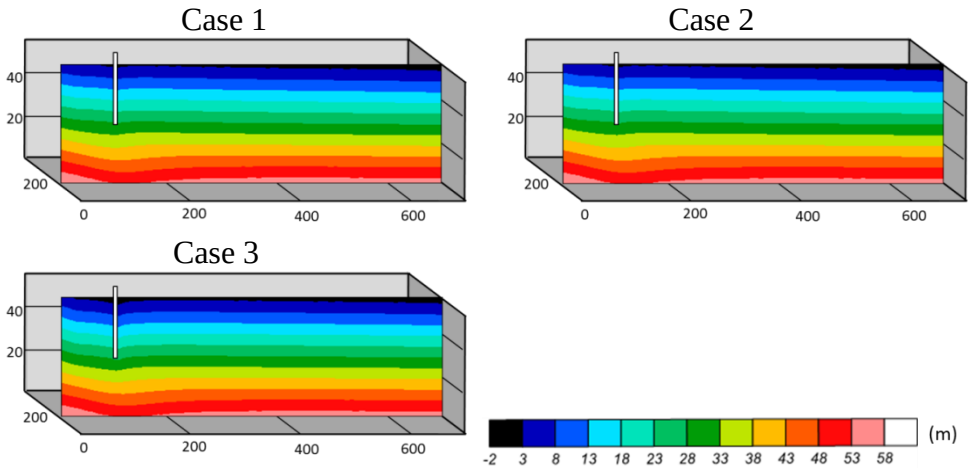

Figure 4.7 Cross-section views of pressure head in the three cases for 2030

Figure 4.8, 4.9 and 4.10 illustrate the cross-section views of the salinity distributions along the pumping well P3 in the three cases for 2011, 2020 and 2030. All figures depict saltwater intrusion into the freshwater aquifer from the seaside boundaries. The salinity levels in Case 1 and Case 2 are nearly same for all these years. On the other hand, the result in Case 3 shows different salinity levels at some positions.

Although upcoming phenomena can generally be seen near wells, the phenomena are significant at the positions approximately 400 m away from the mountainside boudaries for the all cases in 2011 as shown in Figure 4.8. This is probably because the salinity levels around the wells are not high enough to cause an up-coning phenomenon around the well. However, the results show the noticeable up-coning phenomenon around the well in Case 3 for 2020, and 2030 since the doubled groundwater pumping draws more saltwater into the freshwater aquifer.

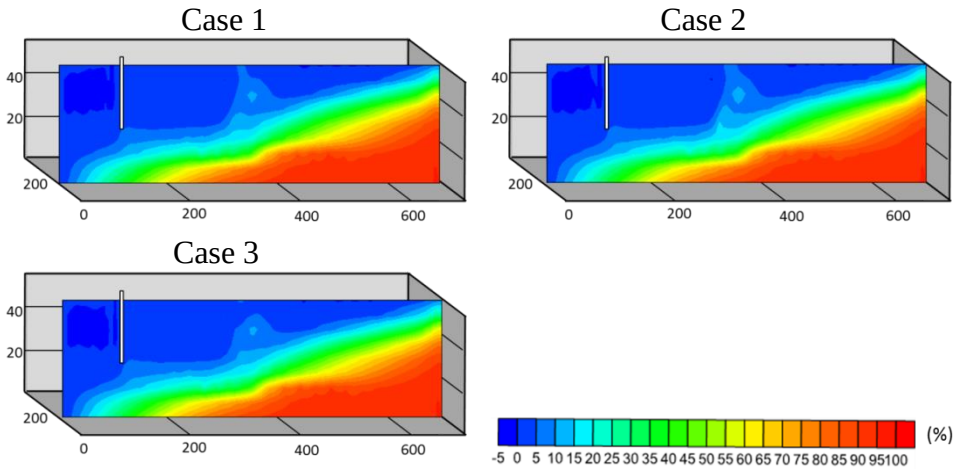

Figure 4.8 Cross-section views of salinity distributions for 2011 in the three cases

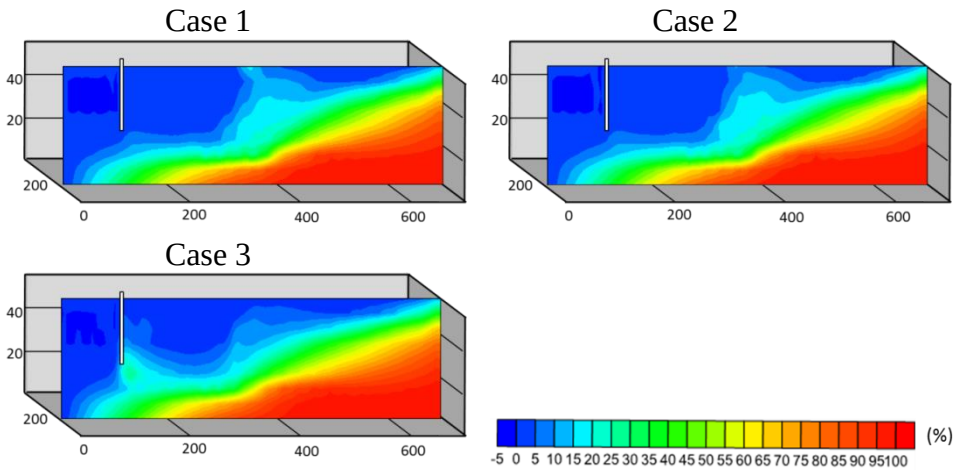

Figure 4.9 Cross-section views of salinity distributions for 2020 in the three cases

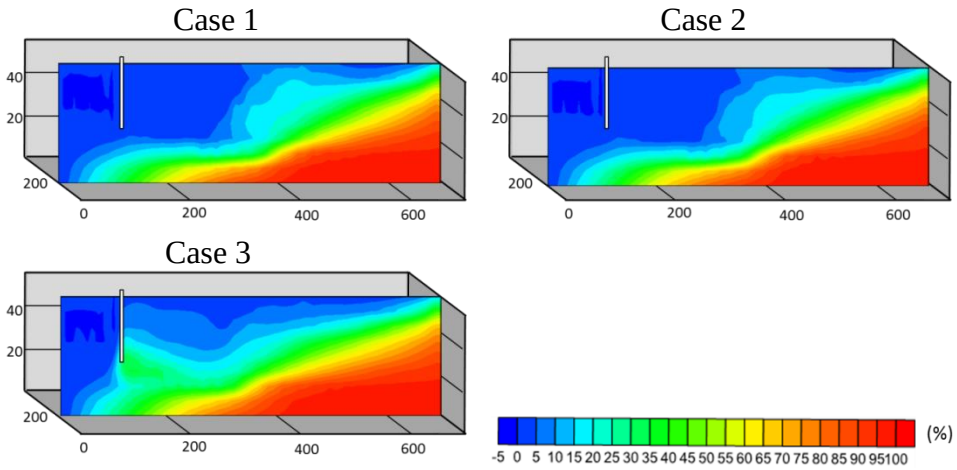

Figure 4.10 Cross-section views of salinity distributions for 2030 in the three cases

Figure 4.11 shows the comparison of the electric conductivities in the three cases at the pumping wells P1, P2 and P3, respectively. At all the wells the electric conductivities in Case 3 are higher than that in Case 1 and 2. This explains that the increase in groundwater discharge has more influence on electric conductivity than the land-use change. The electric conductivity in Case 3 becomes more than 3000 µS/cm at the well P3 while the value in Case 3 reaches only 100 µS/cm at highest at the well P1 and P2 in 2030. The rise of the electric conductivity due to the higher groundwater pumping rate at the well P3 is considerably larger than the wells P1 and P2. Although the pumping wells are gathered, the well P3 is closer to the seaside boundary. Therefore, the well P3 is more vulnerable to saltwater intrusion than the other wells. Since the well P3 pumps up water with high salinity levels, the influences of the doubled groundwater discharge rates are significant at P3. The water with high salinity levels is pumped up by the well P3 and therefore does not reach the well P1 and P2, resulting in little influence on the electric conductivities at the well P1 and P2.

The electric conductivities at pumping wells depend on positions of well screens. If well screens are at high positions, the water pumped up from the well has lower salinity level. As the exact positions of the well screens of the three pumping wells are unknown, the electric conductivity values at the pumping wells may not be reliable. However, the tendencies of the electric conductivities in the all cases do not change with the positions of the well screens.

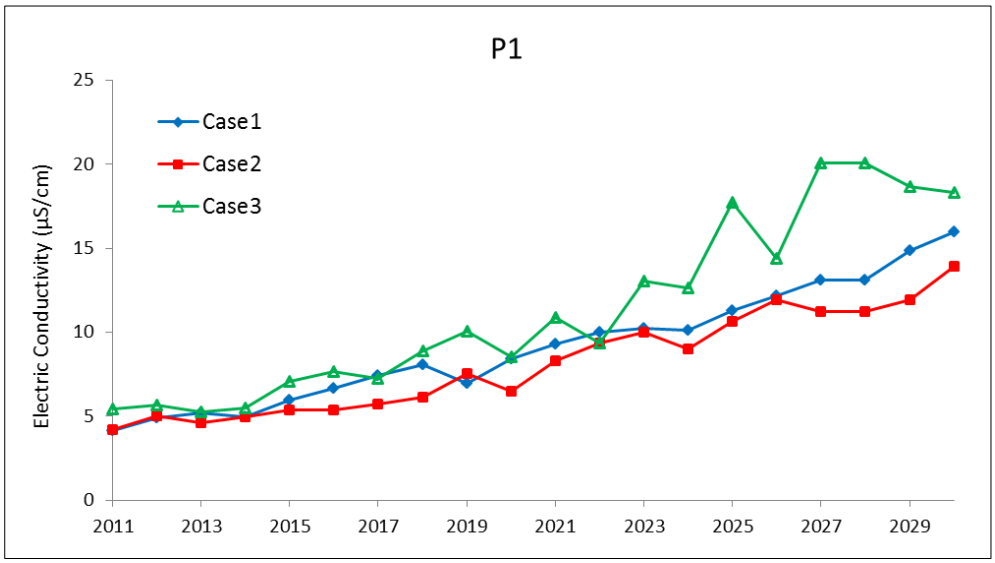

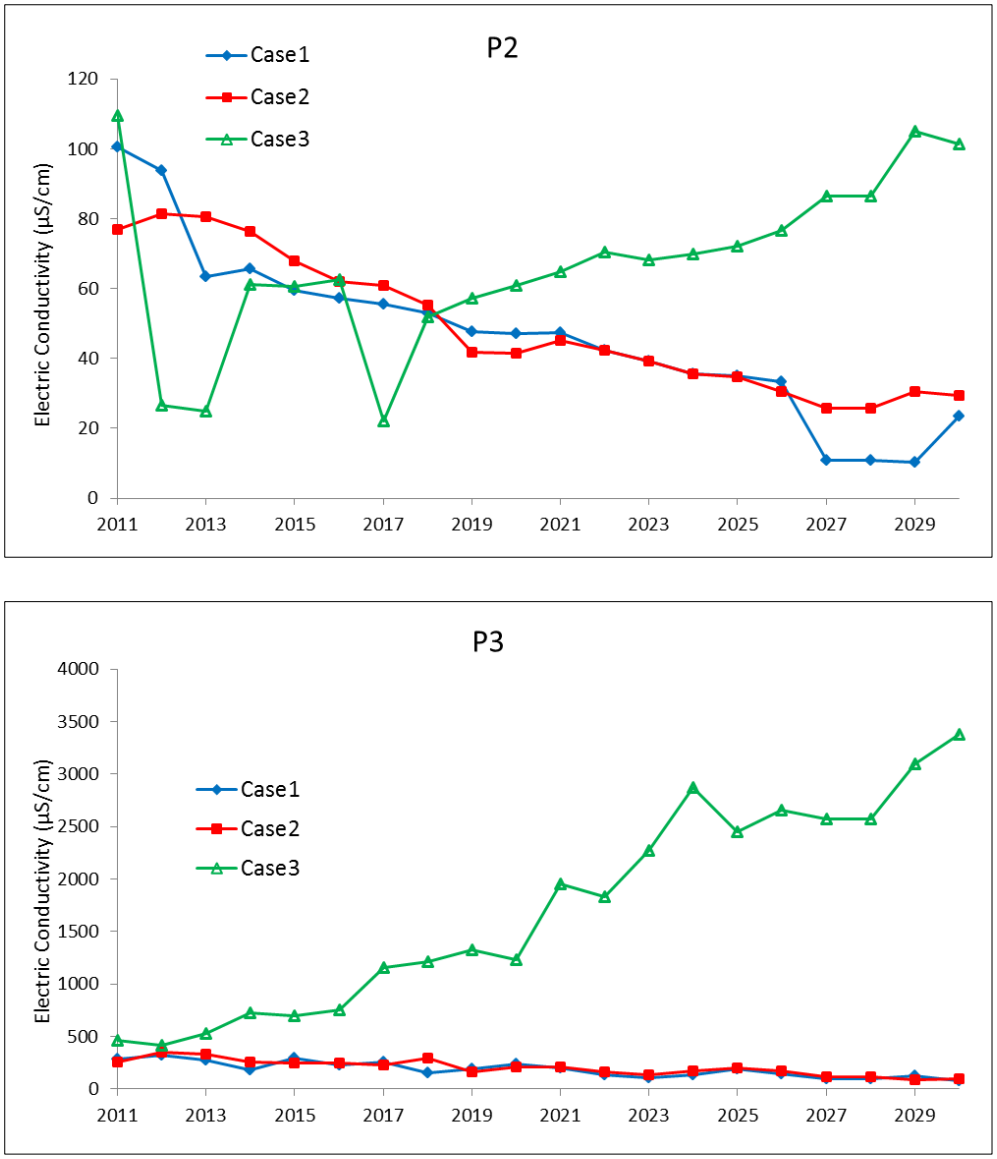

Figure 4.11 Electric conductivities in the three cases at the well P3 from 2011 to 2030

The results show the effect of doubling groundwater pumping rates on saltwater intrusion is larger than that of the land-use change. The effects of lower pumping rates than Case 3 are presented below. The pumping rate in Case 1 is increased by 25 percent and 50 percent and the results are added to Figure 4.11. Figure 4.12 shows the electric conductivities at the well P3 in the three cases and when pumping rate is increased by 25 percent and 50 percent. This figure explains the increase in pumping rate has a more impact than the land-use change even if the increase is less than Case 3.

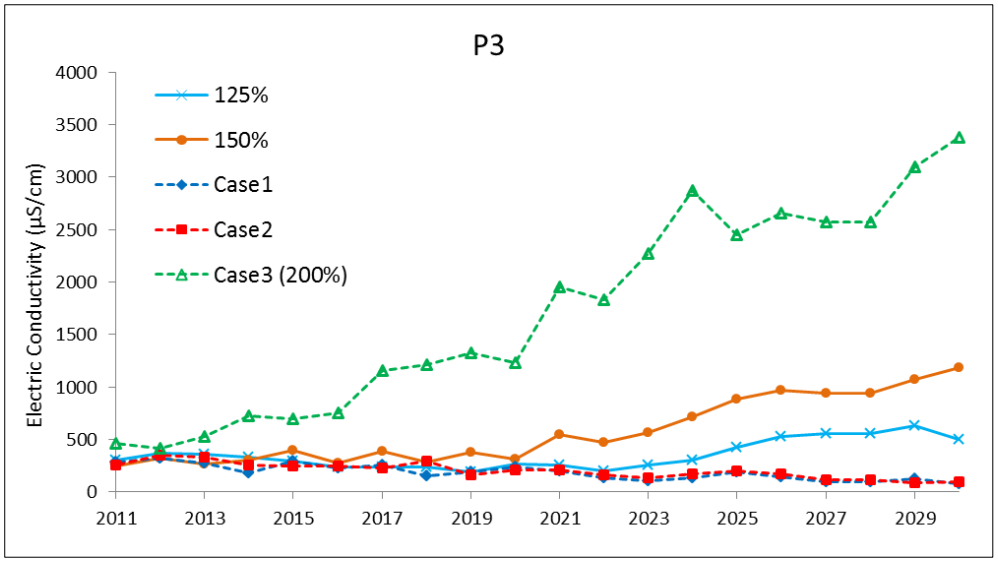

Figure 4.12 Electric conductivities with increased pumping rates and in the three cases from 2011 to 2030

4.3 Discussions

The reasons why the land-use change rarely affects saltwater intrusion in the study area are discussed in this part.

4 points are selected randomly and used to compare the calculated groundwater levels in the three case. Figure 4.13 shows the selected points and Figure 4.14 describes the comparisons of groundwater level in the three cases. The differences of groundwater levels in Case 1 and 2 at CWL 2, 3 and 4, which can be considered as the lowering of groundwater level due to the land-use change, are less than 0.2 m. Although the lowering of groundwater level is nearly 0.5 m at CWL1, the salinity level of the water around CWL1 is very low and therefore it is unlikely that the lowering have an great impact on saltwater intrusion. The lowering of groundwater level due to the land-use change is not significant where the lowering can enhance saltwater intrusion.

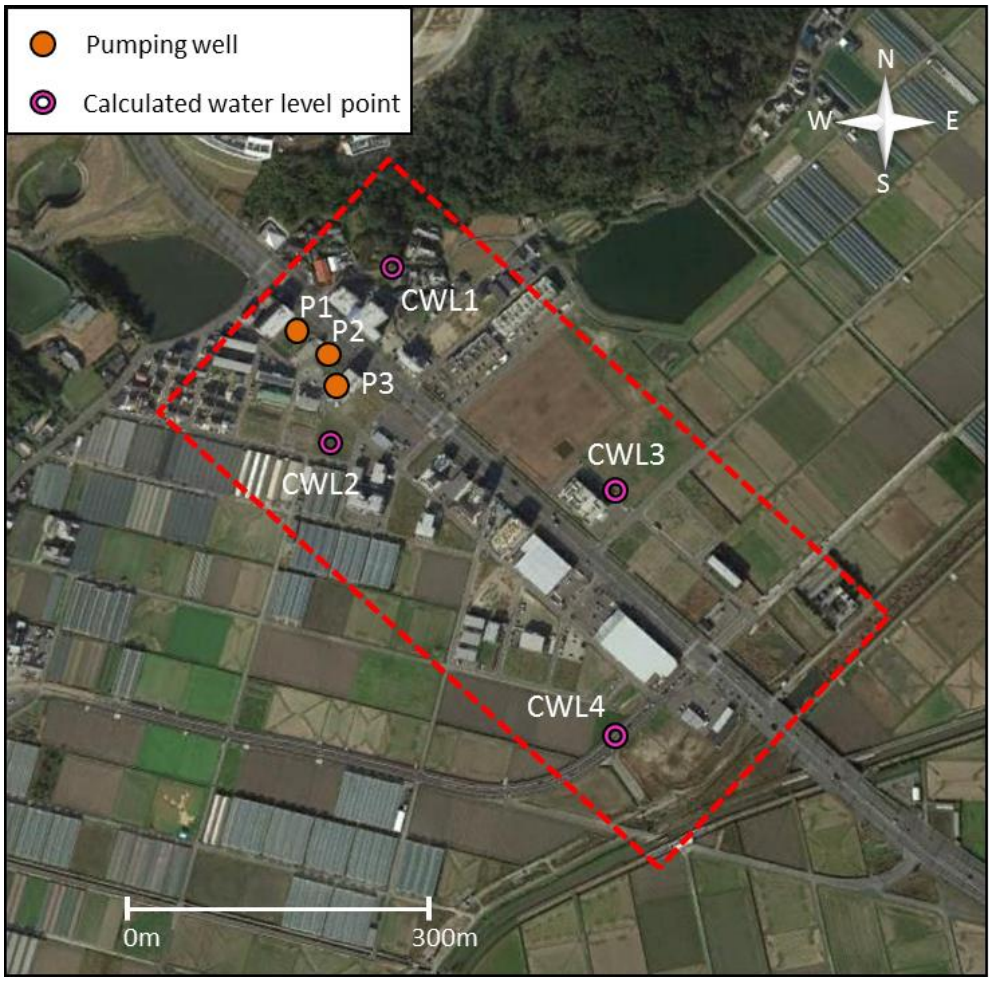

Figure 4.13 Location of the calculated groundwater level points

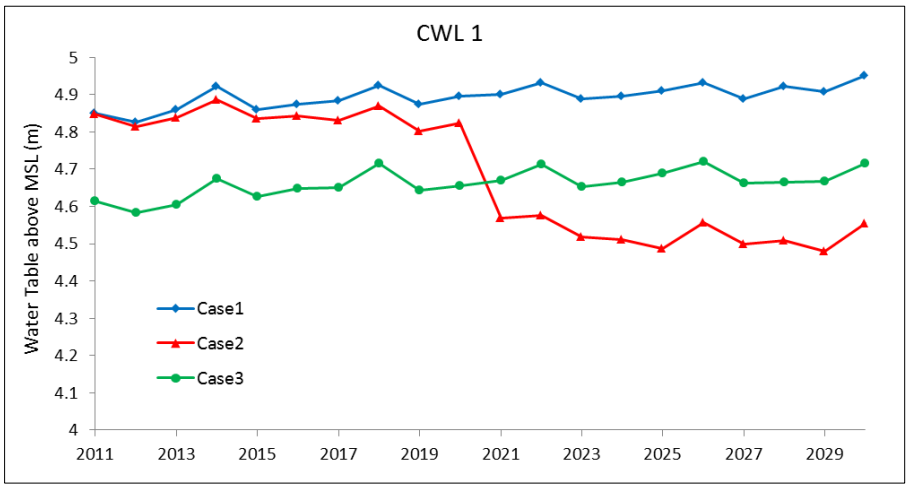

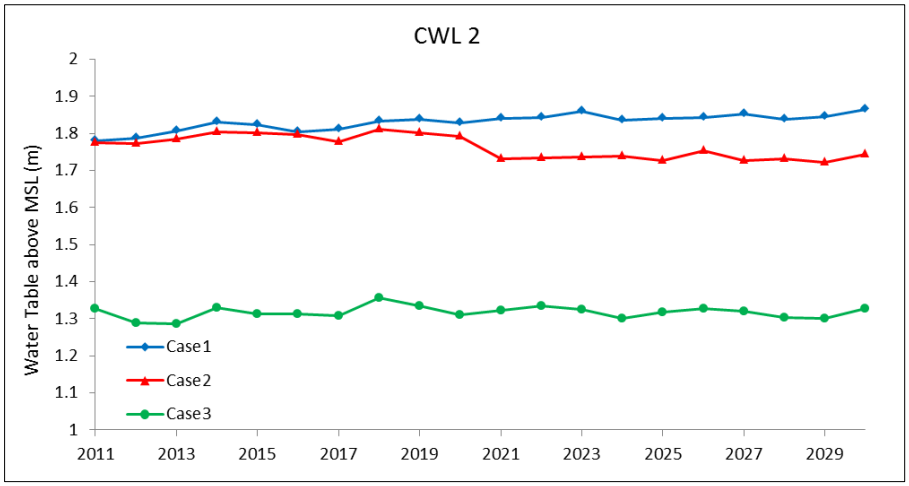

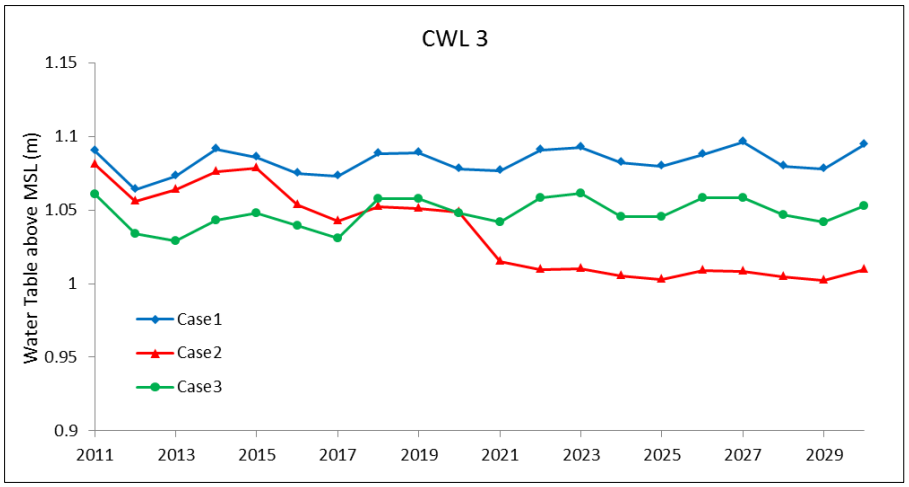

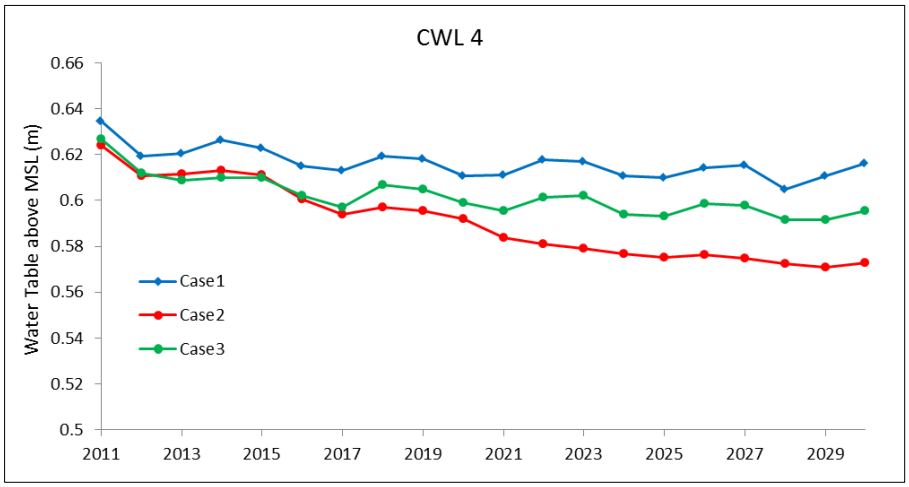

Figure 4.14 Calculated groundwater levels at the selected points

The main reason why groundwater level is not lowered significantly due to the land-use change is high recharge rates in the surrounding area. The surrounding area still has high recharge rates after the land-use is changed and the recharge rate reaches nearly zero. The recharged water in the surrounding area flows towards the study area and prevents the drastic lowering of groundwater level. Figure 4.15 explains groundwater flowing towards the study area from the side of the area in Case 2.

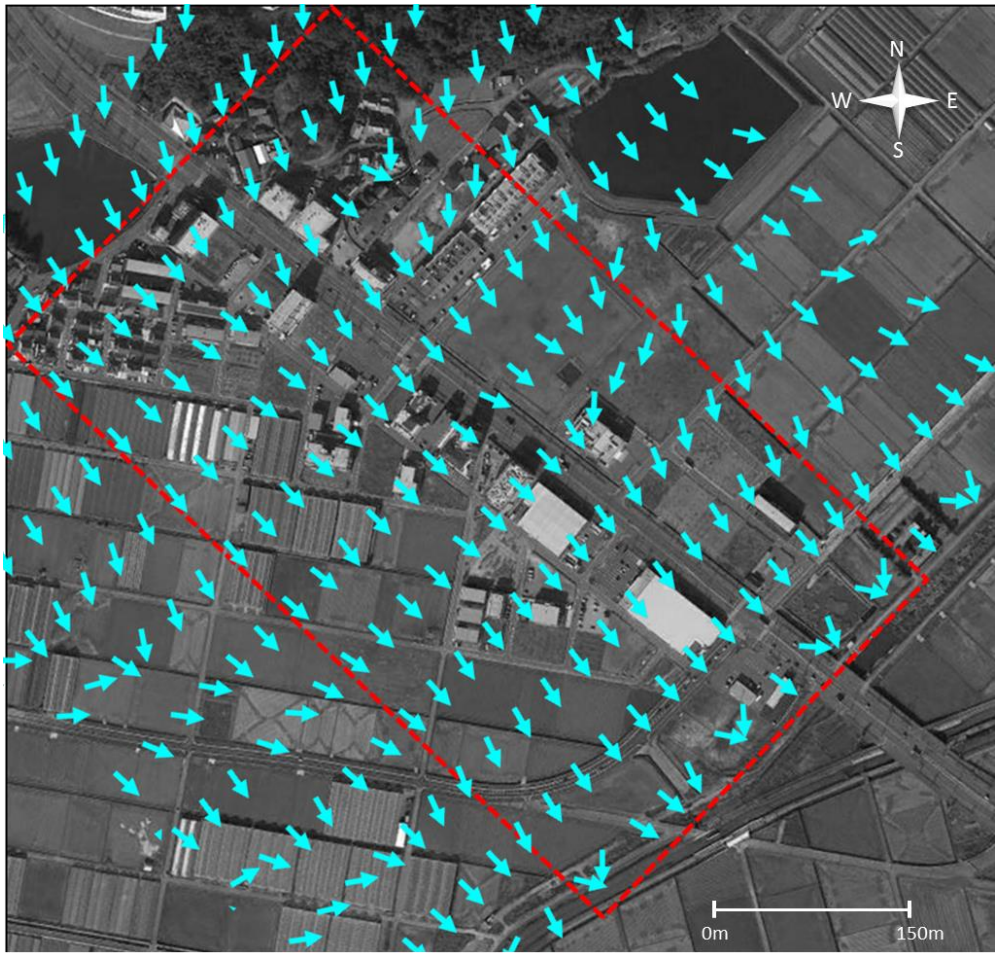

Figure 4.15 Simulated groundwater flow around the study area in Case 2

The lowering of groundwater level in Case 3 is smaller than Case 2 at the points other than CWL2. This explains the lowering of groundwater level caused by the land-use change is larger than groundwater pumping in the most part of the study area. However, the salinity level in Case 3 is considerably higher than Case 2.

The reason can be that the lowering of groundwater level due to the decrease in recharge rate occurs uniformly in the whole area whilst the lowering due to pumping is larger near the pumping wells and get smaller as it is further from the well (Figure 4.16). The uniform lowering rarely reduces the seaward hydraulic gradients. Since velocities are proportional to hydraulic gradients, velocities can also be maintained if hydraulic gradients are maintained. When seaward velocities are not affected, saltwater does not intrude into the freshwater aquifer easily (Maderi, M.N., 2013). On the other hand, the lowering of groundwater level caused by higher pumping rates reduces the seaward hydraulic gradients and hence velocities, which enhances more saltwater intrusion.

Figure 4.17 shows the illustration of the relationships between seaward hydraulic gradients and saltwater intrusion. As shown in the top figure of Figure 4.17, small seaward hydraulic gradient reduces seaward velocities, leading to allowing saltwater intrusion into freshwater aquifer. However, if large seaward gradient is maintained, seaward velocity can block the intrusion.

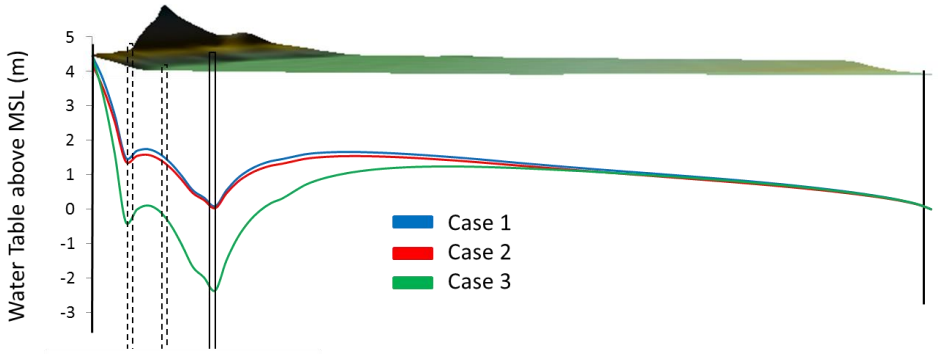

Figure 4.16 Cross-section view of groundwater table above MSL along the well P3in 2030 in the three cases

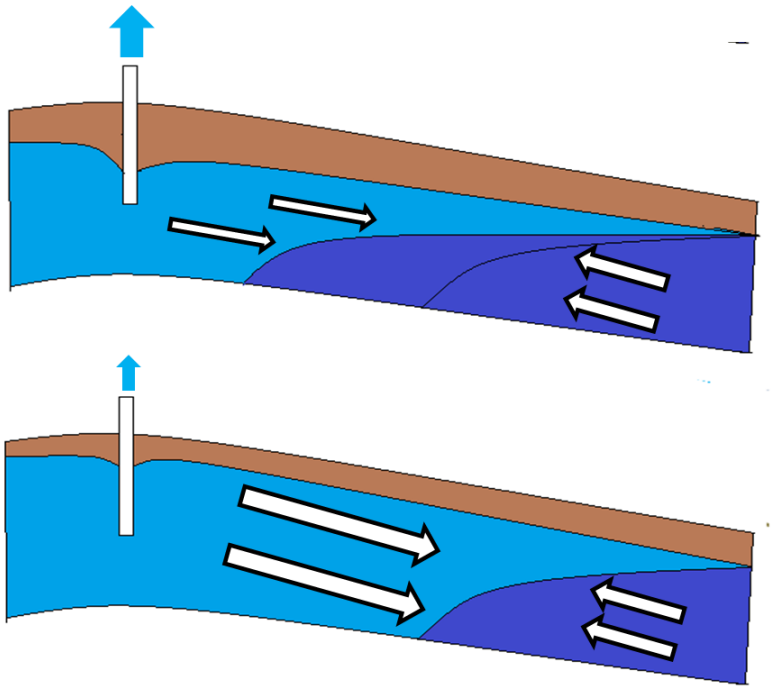

Figure 4.17 Relationships between hydraulic gradients and saltwater intrusion

4.4. Sensitivity analysis

Sensitivity analysis indicates the sensitivity of hydraulic parameters to the simulation results. In this simulation, the hydraulic conductivities of the aquiclude and the aquifer, and the dispersion length are analyzed. When the hydraulic conductivities are increased, higher salinity level is seen in the whole area and the electric conductivity in the pumping wells becomes higher. It is found that the increased hydraulic conductivities of the aquiclude and the aquifer encourage more saltwater into the freshwater aquifer system. When the higher dispersion length is used, the salinity level is increased and wider mixing zone is found.

5. Conclusions

In order to evaluate the effects of groundwater pumping and land-use change on saltwater intrusion in the study area, the simulations in the three cases are conducted by applying groundwater recharge model three dimensional density dependent solute transport model. In the validation period, the observed data and the results from the simulation show reasonable correlations.

The numerical results in the estimation period demonstrate that the salinity level in the case that the land-use is changed (Case 2) rarely increases while that in the case that the pumping rate is doubled (Case 3) increases significantly around the pumping wells.

It is concluded that the effect of land-use change on the extent of saltwater intrusion is much smaller than that of groundwater pumping.

Here are some reasons to consider:

- The groundwater level is not lowered significantly since the surrounding area still has high recharge rates and hence groundwater flowing from the surrounding area prevents drastic lowering of groundwater level in the study area.
- The decrease in groundwater recharge rates due to the land-use change lowers groundwater level uniformly, which rarely reduces the seaward hydraulic gradient and velocity. On the other hand, the high rates of groundwater pumping have great influences the water level around the pumping wells. This reduces the seaward hydraulic gradient and velocity, leading to allowing saltwater intrusion.

The calculated electric conductivity affected by the land-use change does not rise until 2030 in the pumping wells, which explains that it is unlikely that the land-use change in this area will increase the extent of saltwater intrusion in the future. To prevent the extent of saltwater intrusion, we need to pay more attention to the groundwater pumping rates than the land-use change.

References

Abderson, M.P. & Woessner, W.W. (1992) Applied Groundwater Modelling simulation of Flow and advective Transport. Academic Press, San Diego, Calfornia.

Barlow, P.M. (2003). Ground water in freshwater-saltwater environments of the Atlantic Coast. U.S. Geological Survey Circular

Barlow, P.M. & Reichard, E.G. (2010). Saltwater intrusion in coastal regions of North America, Hydrogeology Journal 18, pp247-260

Bear, J. & Verruijt, A. (1997) Modeling groundwater flow and pollution. D. Reidel Publishing Company, Dogrecht, Holland

Bouwer, H. (1978) Towards a new paradigm in hydrology. In: Water flor the Future: Hydrology in Perspective (Proc. Rome Symp., April, 1987), 393-403. IAHS Publ. 164

C.W. Fetter, Jr. (2001) Applied Hydrology, Fourth Edition, Pearson Prentice Hall, USA

Dierch, H.J.G. & Kolddítz, O. (2002), Variable-density flow and transport in porous media: approaches and challenges. Advances in Water Resources, Vol. 25, pp.899-944.

Fukushuma, Y. & Suzuki, M. (1987) Long-term and short-term hybrid runoff model for small mountain catchment. Research Report of Water Resources 7, 35-52

Johnson, R.C. (1990) The interception, throughfall and stemflow in a forest in Highland Scotland and the comparison with other upland forests in the UK. J. Hydrol. 118, 281-287

Konishi, K. (2016) Estimation of amount of groundwater pumping discharge and its effect on salinization of groundwater around Ito Campus, Kyushu University. Memoirs of the faculty of engineering, Kyushu University, Vol. 76, No.1, pp.1-18

Klaassen, W., Lankreijer, H.J.M. & Veen, A.W.L. (1996) Rainfall interception near a forest edge. J. Hydrol. 185, 349-361

Kondo, J., Nakazono, S., Watanabe, T. & Kuwagata, T. (1992) Hydrological climate in Japan (3), Evapotranspiration from forest. J. Japan Soc. Hydrol. Water Resour. 5(4), 8-18

Leyton, L., Reynolds, E.R.C., Thompson, F.B. (1967) Rainfall interception in forest and moorland. In: Forest evapotranspiration. Nordic Hydrol. 6, 70-88

McCuen, R.H. (2004.) Hydrologic Analysis and Design. Prentice Hall, New Jersey.

Naderi, M.N., Kermani, M.R.H. & Barani, G.A. (2013) European Journal of Experimental Biology. 3(3):80-94

Ogawa, S., Ootsuki, K., Hirose, S., Kumagai, T. & Takeuchi, S. (2001) Construction of integrated model for quantification of water volume, mass, quality, and energy in forests.

Perera, E.D.P. (2010). Numerical simulation of hydrogeological and biogeochemical characteristics of coastal subsurface environments, Master thesis of Institute of Urban and Environmental System Engineering Faculty of Engineering, Kyushu University

Research Report for Scientific Research Fun, no. 10306009, 70-73.

Sato, K. & Iwasa, Y. (2003). Groundwater hydraulics. Springer, Tokyo.

Tsutsumi, A., Jinno, K. & Berndtsson, R. (2004) Surface and subsurface water balance estimation by the groundwater recharge model and a 3-D two-phrase flow model. Hydrological Sciences-Journal-des Sciences Hydrologiques 49(2), 205-226.

Van Genuchten. (1980). A closed-form equation for predicting the hydraulic conductivity of unsaturated soils. Soil Science Society of America Journal, Vol. 44, pp.893-898.

Ven Te Chow (1964) Handbook of Applied Hydrology. McGraw-Hill, New York

Water treatment solutions Lenntech BV, Rotterdamseweg 402 M, 2629 HH Delft, The Netherlands, http/www.lenntch.com

Weixing, G. & Christian, L.D. (2002) User's guide to SEAWAT: A computer program for simulation of three dimensional variable density groundwater flow. Tallahassee, Florida, USGS.